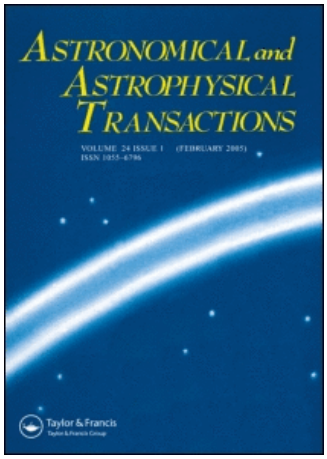

Astronomical & Astrophysical Transactions
The Journal of the Eurasian Astronomical Society
Publication details, including instructions for authors and subscription information:
http://www.informaworld.com/smpp/title~content=t713453505

A gaseous disk in external barred potential: Angular momentum and mass transfer

V. V. Levy [a]; V. V. Mustsevoy [a]; V. A. Sergienko [a]
[a] Volgograd University, Volgograd, Russia

Online Publication Date: 01 November 1996
To cite this Article: Levy, V. V., Mustsevoy, V. V. and Sergienko, V. A. (1996) 'A gaseous disk in external barred potential: Angular momentum and mass transfer', Astronomical & Astrophysical Transactions, 11:1, 1 - 38
To link to this article: DOI: 10.1080/10556799608205452
URL: http://dx.doi.org/10.1080/10556799608205452

Astronomical and Astrophysical Transactions, 1996, Vol. 11, pp. 1–38
Reprints available directly from the publisher
Photocopying permitted by license only

A GASEOUS DISK IN EXTERNAL BARRED POTENTIAL: ANGULAR MOMENTUM AND MASS TRANSFER

V. V. LEVY, V. V. MUSTSEVOY, and V. A. SERGIENKO

Volgograd University, Volgograd, Russia

(Received April 20, 1993)

The evolution of the gaseous disk of a flat galaxy in the field of external gravitational potential of stellar disk, spheroidal component and rotating bar-like perturbation is simulated. The bar-like perturbation amplitude is growing from zero up to some cut-off value and does not change thereafter.

It is shown that with rapidly growing bar such disk passes through two stages of evolution. In the first one the mass and angular momentum redistribution (following the density spiral wave generation by bar potential) leads to dynamic separation of the central and peripheral regions of the disk. In the second stage a quasi-periodic process sets up. During every quasi-period there occur consequently: a superposition of two-armed spiral wave and perturbation ring moving outwards; a distortion of the spiral perturbation into a ring; the stop of the resulting ring-like perturbation and the development of the inward motion which reflect at the outer Lindblad resonance.

The angular momentum and mass transport and physical mechanisms governing quasi-periodic process are analyzed in detail. A possible application of the results obtained to the interpretation of the dynamics of SB galaxies is discussed.

KEY WORDS Gas dynamics, numerical simulation, barred galaxies

1 INTRODUCTION

A detailed investigation of the dynamics of angular momentum and mass transfer in gaseous disks is important for modelling of evolution of flat galaxies as well as for a correct treatment of observational data for such objects. On the one hand, if the transport mechanisms are effective, the observed distributions of angular momentum in galactic disks are not steady, and may greatly differ from those existed at any previous stage of evolution (Gorbatsky, 1986; Saslaw, 1987). On the other hand, a number of investigators pointed out that rotation curves and gas surface density distributions are determined not only by the radial equilibrium of centrifugal and gravitational forces, but also by some dynamic effects caused by momentum transfer (e.g. Lynden–Bell and Kalnajs, 1972; Morozov *et al.*, 1985c).

In galactic gaseous disks the viscosity and nonaxisymmetric density waves can redistribute angular momentum rather effectively, and besides, such redistribution

may be caused by nonaxial symmetry of gravitational potential (due to tidal interaction, development of stellar spiral or bar modes, etc.). The two latter mechanisms are closely related to each other, since nonaxisymmetric potential inevitably leads to the generation of gas density waves in potential wells of stellar density waves (Roberts, 1963; Marochnik *et al.*, 1983; Kovalenko and Levy, 1992).

Momentum exchange due to interactions of interstellar gas clouds largely governs viscous transport of angular momentum in stellar-gaseous disks in the absence of spiral density waves (Gorbatsky, 1986). Typical parameters of the cloud motion (with mass of about $100M_{\odot}$), the "free path length" between "collisions", the number of collisions during the life time, etc., allow to describe this process quite well with collisional viscous perfect gas equations, clouds being treated as gas particles (molecules)†. A number of numerical experiments (Gorbatsky and Serbin, 1983; Gorbatsky and Usovitch, 1986) were performed, where a gaseous disk with parameters close to those of the Galaxy was investigated. Their calculations showed that the radial gas flows constant in direction arise due to angular momentum transport from inner regions of the disk to outer ones. These flows are directed inwards in the inner regions and outwards in the outer, the latter leads to a considerable growth of the outer radius of the disk. In the typical time of $5 \times 10^8 \div 10^9$ years as much as several tenths of the total gas mass flows out through this radius. Besides, the nonuniformity of radial velocities produces significant local maxima of gas surface density.

Similar consideration of the gas of giant molecular clouds (mass of about $10^5 \div 10^6 M_{\odot}$) treated as molecules shows that such gas exhibits some viscosity due to gravitational interaction of the clouds, though being collisionless (Gorbatski and Serbin, 1983; Fukunaga, 1983). Their numerical simulations demonstrate how the initially uniform distribution of GMC produces a ring similar to that being observed with a density maximum at a radius of 5 kpc.

Angular momentum transport associated with the dynamical friction of GMC upon stellar disk was discussed by Surdin (1980), Lipunov (1982), Sil'chenko and Lipunov (1987a, 1987b) in the model of collisionless gas of GMC. Sil'chenko and Lipunov (1987b) also included viscosity.

A spiral density wave can transfer angular momentum in a stellar disk (Lynden-Bell and Kalnajs, 1972) as well as in a gaseous one (the latter was extensively investigated in application to accretion disks – see, e.g. Papaloizou and Pringle, 1985, 1987; Glatzel, 1987; Savonije and Heemskerk, 1990; Papaloizou and Savonije, 1991). The understanding of the origin of excitation and support of global nonaxisymmetric modes is of crucial significance for analysis of the problem. In the gaseous disks the stellar density wave (gas feels it as a gravitational potential well – Roberts, 1969; Marochnik *et al.*, 1983; Kovalenko and Levy, 1992), or the hydrodynamic instabilities due to self-gravity (e.g. Papaloizou and Savonije, 1991) or produced by the radial gradients of the disk parameters (Fridman, 1978) may be of that origin. These instabilities, in turn, may be caused by:

† The concept of viscosity for such a gas was introduced by Mishurov *et al.* (1976) in their study of galactic disk stability.

(i) an unstable distribution of mass forces acting upon the "fluid particles" at any deviation from initial equilibrium condition of the disk (the gravitational, groove, centrifugal, "strong" dissipative, entropygradient and other instabilities – see, e.g., Papaloizou and Savonije, 1991; Morozov 1977, 1979, 1989; Fridman, 1990; Baev, 1989; Morozov *et al.*, 1986; Levy and Morozov, 1989; Morozov and Hoperskov, 1990);

(ii) action of surface forces (Kelvin–Helmholtz instability that is due to the Bernoulli effect – Fridman, 1990; Morozov *et al.*, 1986);

(iii) resonant interaction between the wave and the basic flow in the vicinity of the corotation radius, where their angular velocities coincide, or/and between the modes with different signs of energy density localized on either side of the corotation (Papaloizou and Pringle, 1985, 1987; Glatzel, 1987; Savonije and Heemskerk, 1990; Papaloizou and Savonije, 1991; Glatzel, 1990).

Of course, excitation by a combined mechanism (the groove-centrifugal – Fridman, 1990, and the resonant-centrifugal – Morozov *et al.*, 1992, etc.) is possible. Note that the character of the redistribution of material and angular momentum depends crucially on the specific mechanism of the spiral wave development (cf. Mustsevoy and Prokhorov, 1992).

Angular momentum transfer in rotating disk systems with nonaxisymmetric gravitational potential was often considered in application to tidal interaction in stellar galactic (Toomre 1977, 1981) and gaseous accretion (e.g. Sawada *et al.*, 1987; Larson, 1988; Spruit, 1989) disks, i.e. with a perturbation source lying away from the disk, and, consequently, its influence was maximal at one side of the disk and minimal at the opposite side. Besides, angular momentum exchange (dynamic friction) between the bar potential and stellar galactic disk was studied by Little and Carlberg (1991).

We think it to be rather interesting to investigate the dynamics of angular momentum redistribution in gaseous disk in the field of a rotating nonaxisymmetric stellar bar. Our attention to this model is caused by the following considerations. We guess that some interesting effects may be revealed in this model such as a resonance between the wave of potential and eigenmodes of the gaseous disk, excitation of hydrodynamic gradient instabilities by finite amplitude perturbations, etc., and we expect the mass and angular momentum transport to be significantly more efficient and occur at shorter typical times than in the case of self-amplification and self-support of perturbations growing from a linear stage. Finally, the data on the evolution of disk parameters and spiral structure obtained in experiments with a model like that may be very useful in interpretation of processes taking place in SB galaxies.

Note that numerical experiments with a similar model were performed earlier, but the objects of study were either the spiral pattern development and evolution (see Athanassoula, 1980; Korchagin and Shevelev, 1980, 1981; van Albada and Sanders, 1982; Roberts and Haustman, 1984; Matsuda *et al.*, 1987) or the gas

dynamics in the central part of the disk, the inflow and outflow rates in the galactic nucleus region (Athanassoula, 1988; Afanas'ev *et al.*, 1989)†.

This paper appeared as a result of combination of two approaches to gas disk investigation. The numerical experiments performed by VVL with different aimes (see footnote 2) gave a lot of data that confirmed the theoretical results obtained by VVM.

In Section 2 we formulate the problem and give the model description and basic equations. Section 3 describes the method of numerical experiment and the values of parameters used. The results are analyzed in detail in Section 4, and Section 5 is devoted to possible astrophysical applications.

2 THE MODEL AND BASIC EQUATIONS

We consider the evolution of a gaseous disk rotating in an external gravitational field simulating the stellar subsystems of a flat galaxy – a spherically symmetric (halo and corona) and axisymmetric (disk). Not-axisymmetric component simulating the excitation of stellar bar-mode grows smoothly and comes to a fixed amplitude (nonlinear saturation).

2.1 The Gravitational Potential

The surface density distribution in the stellar disk is assumed to be exponential:

$$\sigma_*(r) = \sigma_{*0} \exp(-r/L_\sigma), \tag{1}$$

where r is the distance from the disk axis of rotation, L_σ is the typical length scale of surface density. Hence the total mass of the disk is $M_D = 2\pi\sigma_{*0}L_\sigma^2$, its contribution to the gravitational potential of the system is the following:

$$\psi(r) = \frac{GM_D}{L_\sigma}\left[\frac{r}{L_\sigma} I_1\left(\frac{r}{2L_\sigma}\right) K_0\left(\frac{r}{2L_\sigma}\right) - 1\right], \tag{2}$$

here $I_1(x)$ and $K_0(x)$ are the modified Bessel functions, G is the gravity constant.

The distribution of volume density of the spherical component is assumed to been

$$\varrho_*(s) = \varrho_{*0}/(1 + s^2/R_H^2), \tag{3}$$

where $s = (r^2 + z^2)^{1/2}$ is the distance from the center of the system, R_H is a typical size of the halo core. In order to calculate the potential of halo correctly we have to scale it in such a way that $\psi_H(s) \to 0$ at $s \to \infty$. Besides, since it is spherically symmetric and the numerical grid is finite we may assume $\varrho_*(s > r_{\max}) = 0$, where $r_{\max}$ is an outer boundary of the numerical grid.

†In this paper we do not discuss the processes in the central (close to nucleus) part of the disk, since they are objects of special consideration (Levy, 1993).

The axisymmetric potential in the plane of the gaseous disk,

$$\psi(r, t = 0) \equiv \psi_0(r) = \psi_D(r) + \psi_H(r), \tag{4}$$

is disturbed by a bar-like perturbation, so that the total potential of the system is

$$\psi(r, \varphi, t) = \psi_0(r) \{1 + \varepsilon(r, t) \cos[2(\varphi - \Omega_B t)]\}, \tag{5}$$

where Ω_B is the bar angular velocity, and the amplitude function of the perturbation is

$$\varepsilon(r, t) = \varepsilon_0 A(t)(r/a)^2[1 + (r/a)^2]^{-3/2}, \tag{6}$$

where

$$A(t) = \begin{cases} 0, & \text{if } t < 0, \\ \sin^2\left(\frac{\pi}{2}\frac{t}{\tau_B}\right), & \text{if } 0 \le t \le \tau_B, \\ 1, & \text{if } t > \tau_B, \end{cases} \tag{7}$$

ε_0 is the "bar amplitude", τ_B is its typical time-scale. The typical length-scale of the bar a is taken as the length unit hereafter.

2.2 The Model of the Gaseous Disk

We neglect self-gravity of the gaseous disk, i.e. we assume its mass to be small, so that the redistribution of mass during the disk evolution cannot affect the gravitational potential of the system. Besides, we suppose that the total mass of the gas in the disk M_G is conserved (that is, star formation and cloud formation of gas ejected by stars balance each other). We assume the initial gas density distribution to be exponential: $\sigma(r, t = 0) = \sigma_0 \exp(-r/L_\sigma)$, and internal energy per mass unit to be constant: $e = \text{const}$. It means that the disk is initially isothermal and may be described by equation of state for perfect gas:

$$p = (\gamma - 1)\sigma e, \tag{8}$$

where p is the two-dimensional gas pressure, γ is the two-dimensional specific heats ratio.

Following Churilov and Shukhman (1981), we assumed $\gamma = 3/2$. Note, by the way, that the applicability of Eq. (8) with such a value of γ to a gas of cloud-macromolecules has observational evidence besides theoretical results of Churilov and Shukhman (1981). Indeed, in a polytropic gas the surface density and sound speed c_s (for the latter the dispersion of interstellar gas cloud velocities assumes) are not independent but are related (see, e.g. Fridman, 1990) as $c_s(r_1)/c_s(r_2) = [\sigma(r_1)/\sigma(r_2)]^{(\gamma-1)/2}$, where r_1 and r_2 are arbitrary radii. At the same time, observations show (Sanders *et al.*, 1984) for the solar neighborhood ($r_\odot \approx 10$ kpc) that $\sigma_\odot \approx 8 M_\odot/\text{pc}^2$, $c_{s\odot} \approx 8$ km/s, and in the central region ($r_c \approx 1$ kpc) $\sigma_c \approx 600 M_\odot/\text{pc}^2$, $c_{sc} \approx 20$ km/s, which roughly (allowing for observational errors and the fact that in central regions of a real disk the law governing the processes in gas surely differs from the polytropic one) corresponds to the value of $\gamma = 3/2$ and we have no reasons to regard this feature to be specific only for the Galaxy.

We simulate the cooling of the gas of cloud-molecules due to radiative energy losses. Such losses are rather small at $T < T_0 \simeq 10^4$ K and rapidly grow at $T > T_0$. This statement may need some comments for in reality not the gas of cloud-molecules but the diffuse gas radiates. Nevertheless, there is a strong correlation between the value of dispersion of cloud velocities and the gas luminosity, which may be explained with the following considerations (see, e.g., Gorbatski, 1977). First, in colliding clouds shock waves appear accompanied by radiation. This radiation is the more effective, the higher kinetic energy of the relative motion of the gas particles is, which, in turn, grows along with the dispersion of cloud velocities (the direct collisions are rather rare – in average over the disk a cloud suffers one collision during its life time $t_0 \approx 5 \times 10^7 \div 10^8$ – Gorbatski and Serbin, 1983). Second, the mean dispersion of cloud velocities coincides with the sound speed in the rarefied intercloud gas, which corresponds to the temperature of the radiation threshold, $T \approx 10^4$ K. Consequently, when the dispersion exceeds the mean value of $c_s \approx 10$ km/s, the cloud motion in the intercloud medium becomes supersonic and is accompanied by shock waves. Then the cloud is effectively dragged, its energy being transferred to shock waves, which radiate it as usually.

Note that the two described above ways of cooling of cloud-molecule gas are working for the clouds of small mass ($20 \div 300 M_\odot$, e.g., clouds HI and dark clouds – cf. Bochkarev, 1991), and do not work for GMC. The first way fails due to the GMC gas being collisionless, the second one cannot be applied to the clouds of mass $10^5 \div 10^6 M_\odot$ because they cannot be dragged significantly during their life time. Thus, we study not the dynamics of existing GMC, but the possibility of GMC formation from the clouds of small mass (see Section 4.6), following Gorbatski and Usovich (1986).

We suppose the gas motion to be circular at initial time, $V_r(r, \varphi, t = 0) = 0$, and the azimuthal velocity component is determined from radial balance of forces:

$$\frac{V_\varphi^2(r, t = 0)}{r} = \frac{1}{\sigma}\frac{\partial p}{\partial r} + \frac{\partial \psi_0}{\partial r} \tag{9}$$

Since the disk initial condition is isothermal, the relation $dp = (\gamma - 1) e d\sigma$ is valid and it follows from Eq. (9):

$$V_\varphi(r, t = 0) = [r \partial \psi_0 / \partial r - r(\gamma - 1) e / L_\sigma]^{1/2}, \tag{10}$$

The hydrodynamic equations describing the gaseous disk evolution in an inertial frame of reference are the following:

$$\frac{\partial \sigma}{\partial t} + \frac{\partial (r \sigma V_r)}{r \partial r} + \frac{\partial (\sigma V_\varphi)}{r \partial \varphi} = 0, \tag{11}$$

$$\begin{aligned} \frac{\partial (\sigma V_r)}{\partial t} &+ \frac{\partial (r \sigma V_r^2)}{r \partial r} + \frac{\partial (\sigma V_r V_\varphi)}{r \partial \varphi} - \frac{\sigma V_\varphi^2}{r} \\ &= -\frac{\partial p}{\partial r} - \sigma \frac{\partial \psi}{\partial r} + \frac{\partial (r W_{rr})}{r \partial r} + \frac{\partial W_{r\varphi}}{r \partial \varphi} - \frac{W_{\varphi\varphi}}{r}, \end{aligned} \tag{12}$$

$$\frac{\partial(\sigma V_\varphi)}{\partial t} + \frac{\partial(r\sigma V_r V_\varphi)}{r\partial r} + \frac{\partial(\sigma V_\varphi^2)}{r\partial\varphi} - \frac{\sigma V_r V_\varphi}{r} = -\frac{\partial p}{r\partial\varphi} - \sigma\frac{\partial\psi}{r\partial\varphi} + \frac{\partial(rW_{r\varphi})}{r\partial r} + \frac{\partial W_{\varphi\varphi}}{r\partial\varphi} + \frac{W_{r\varphi}}{r}, \tag{13}$$

$$\frac{\partial(\sigma E_0)}{\partial t} + \frac{\partial(r\sigma E_0 V_r)}{r\partial r} + \frac{\partial(\sigma E_0 V_\varphi)}{r\partial\varphi} + \frac{\partial(rpV_r)}{r\partial r} + \frac{\partial(pV_\varphi)}{r\partial\varphi} = \sigma\frac{\partial\psi}{\partial t} + \frac{\partial(rV_r W_{rr} + rV_\varphi W_{r\varphi})}{r\partial r} + \frac{\partial(V_r W_{r\varphi} + V_\varphi W_{\varphi\varphi})}{r\partial\varphi} + \frac{\partial}{r\partial r}\left(r\theta\frac{\partial e}{\partial r}\right) + \frac{\partial}{r\partial\varphi}\left(\theta\frac{\partial e}{r\partial\varphi}\right) + L(e). \tag{14}$$

Here $E_0 = e+\psi+(V_R^2+V_\varphi^2)/2$ is the total gas energy per unit mass, θ is a parameter describing gas thermal conductivity, $L(e)$ is a function assumed for the radiation losses of gas internal energy. W_{rr}, $W_{r\varphi}$ and $W_{\varphi\varphi}$ are the components of the viscous stress tensor.

2.3 Dissipative Effects

It is evident from Eqs. (11)–(14), that we attempt to include explicitly the effects of viscosity and thermal conductivity which act on the gas of clouds.

The viscous stress tensor components in the disk plane can be written in the form

$$W_{rr} = 2\eta\frac{\partial V_r}{\partial r} + (\zeta - eta)\mathrm{div}V, \tag{15}$$

$$W_{\varphi\varphi} = 2\eta\left(\frac{\partial V_\varphi}{r\partial\varphi}\right) + (\zeta - eta)\mathrm{div}V, \tag{16}$$

$$W_{r\varphi} = \eta\left(\frac{\partial V_r}{r\partial\varphi} + \frac{\partial V_\varphi}{\partial r} - \frac{V_\varphi}{r}\right), \tag{17}$$

where

$$\mathrm{div}V = \frac{\partial(rV_r)}{r\partial r} + \frac{\partial(V_\varphi)}{r\partial\varphi}, \tag{18}$$

η and ζ are the two-dimensional coefficients of surface shear and volume dynamic viscosity (related to the corresponding three-dimensional quantities as $\eta \approx \eta_v H$ and $\zeta \approx \zeta_v H$, H being the disk thickness).

We made several test runs using the following values of parameters: $\theta = 2\eta$, $\zeta = \eta = 10^4 \div 10^{-3}\sigma_0 a^2\Omega_B$ (which corresponds to $\eta_v \approx 8 \times (10^2 \div 10^3)$ g cm^{-1} s^{-1} with $H \approx 0.5$ kpc). Furthermore, a series of runs was performed with $\eta = \zeta = \theta = 0$. The comparison of the results of the two series exhibit two features. First, in "nondissipative" simulations an unavodable (for our computational method and grid – see Section 3) numerical viscosity occurs, and, second, it acts qualitatively

and quantitatively similar to the physical viscosity† with $\eta v \approx 3 \times 10^3$ gcm^{-1}s^{-1}. Gorbatski and Serbin (1983) and Gorbatski and Usovich (1986) estimate the value of ηv for the Galactic disk to be at about this value. This allowed us assume $\eta = \zeta = \theta = 0$ in further simulation runs.

When choosing the radiation energy loss function $L(e)$ for Eq. 14 we took into account that cloud drag described in Section 2.2 is not instantaneous but occurs during a finite period. To simulate this process, the following scheme was applied. At every time step the energy at meshpoint where $e(r,\varphi) < e_{\max}$ ($e_{\max}$ corresponds to $T \approx 10^4$ K) was left unchanged, otherwise the mesh "radiated" $\Delta e = \lambda[e(r,\varphi) - e_{\max}]$, where $\lambda \leq 1$ (we adopted $\lambda = 0.5$). Note that in similar models of Athanassoula (1980), Korchagin and Shevelev (1980, 1981), van Albada and Sanders (1982), Roberts and Haustman (1984) and Matsuda *et al.* (1987) the radiation energy losses were neglected.

3 COMPUTATIONAL METHOD

3.1 Computational Metod and Values of Parameters

In our experiments we used the numerical scheme of "large particles" (Belotserkovski and Davydov, 1982) in polar coordinates. The computational grid consisted of $N_r \times N_\varphi$ grid points ($N_r = 150$, $N_\varphi = 90$) and occupied a semicircle due to the obvious bisymmetry of the model. The grid was equally spaced in the φ-coordinate ($\Delta\varphi = \pi/N_\varphi$), the radial spacing was adopted as

$$\Delta r_i = R_L \left\{ \sinh\left[\frac{i+1}{N_r+1}\operatorname{arcsinh}\left(\frac{R_M}{R_L}\right)\right] - \sinh\left[\frac{i}{N_r+1}\operatorname{arcsinh}\left(\frac{R_M}{R_L}\right)\right]\right\}, \tag{19}$$

where i is the meshpoint number ($1 < i < N_r$); $R_L = 1$ and $R_M = 10$. At the center of the grid there was a single circular point with radius of $r_{\min} = 1.986 \times 10^{-2}$. At the outer grid radius $r_{\max} = 10$, the flow across the boundary was forbidden.

The major semi-axis of the bar a was taken as the length unit (see Eq. 6), and the bar rotation period $T_B = 2\pi/\Omega_B$ as the time unit. The model parameters were adopted as $L_\sigma = 3$, $R_H = 1$, $\tau_B = 0.3$, $\tau_B = 1$ or $\tau_B = 3$ in these units. We used a constant time-step $\Delta t = 0.0001$. The mass ratio of the stellar components (halo to disk) was adopted as $M_H/M_D = 0.567$ and we let the gas angular velocity at $r = a$ to be $\Omega(a, t = 0) = 1.9\Omega_B$ throughout all the experiments. Such a value of Ω is motivated by bar-mode stability investigations (Polyachenko and Fridman, 1976) and numerical experiments (Sellwood, 1980; Morozov, 1981; Mikhajlova and Morozov, 1988) showing that the bars excited in central regions of the disks (having a solid body rotation) are saturated rather soon and possess the phase velocity which is about twice lower than the disk angular velocity. The gas internal energy $e = c_s^2[\gamma(\gamma-1)]^{-1}$ at initial moment was chosen in such way that $V_\varphi(r = a) =$

†This fact agrees with all we know about numerical dissipation and dispersion – cf. Fletcher, 1988

$a\Omega(r=a)=20c_s$. Finally, the amplitude of the bar-like distortion of gravitational potential was set according to $\varepsilon_0=0.1$, $\varepsilon_0=0.3$ or $\varepsilon_0=0.5$.

To simplify the estimations of the parameters in dimensional units we give the typical values $a \approx 1 \div 2$ kpc, $\Omega \approx 100$ km s^{-1} kpc^{-1} and $\sigma(r \leq 0.3 \text{ kpc}) \approx (0.5 \div 2) \times 10^3 M_\odot/\text{pc}^2$.

3.2 Interpretation of the Results

When interpreting the numerical results, we used an obvious fact that all the quantities are periodic in azimuthal coordinate. Averaging Eq. (13) over φ, multiplying it by r and representing all the quantities involved as a sum of a mean value $\langle\Phi\rangle$ and perturbation $\Phi' = \Phi - \langle\Phi\rangle$, one can easily obtain a relationship describing the angular momentum balance between the perturbations and the mean gas flow in the disk:

$$\frac{\partial H}{\partial t} + \frac{1}{r}\frac{\partial(rF)}{\partial r} - \frac{1}{r}\frac{\partial(rQ)}{\partial r} = -\varphi - \frac{\partial h}{\partial t} - \frac{1}{r}\frac{\partial(rf)}{\partial r} + \frac{1}{r}\frac{\partial(rq)}{\partial r}, \tag{20}$$

where $H = r\langle\sigma\rangle\langle V_\varphi\rangle$ is the mean angular momentum density of the basic flow and axisymmetric perturbations; $F = r\langle\sigma\rangle\langle V_r\rangle\langle V_\varphi\rangle$ is the mean radial angular momentum flux density of the basic flow and axisymmetric perturbations; $Q = r^2\langle\eta\rangle/\partial\langle\Omega\rangle/\partial r$ is the mean radial angular momentum flux density of the basic flow and axisymmetric perturbations due to dissipation; $h = r\langle\sigma' V_\varphi'\rangle$ is the mean angular momentum density of nonaxisymmetric perturbations; $f = r\{\langle\sigma\rangle\langle V_r' V_\varphi'\rangle + \langle V_\varphi\rangle\langle\sigma' V_r'\rangle + \langle V_r\rangle\langle\sigma' V_r' V_\varphi'\rangle + \langle\sigma' V_r' V_\varphi'\rangle\}$ is the mean radial angular momentum flux density of nonaxisymmetric perturbations; $q = r\langle\eta'\partial\Omega'/\partial r\rangle + \langle\eta'\partial V_r'/\partial\varphi\rangle$ is the mean radial angular momentum flux density due to dissipation of nonaxisymmetric perturbations; $\phi = \langle\sigma'\partial\psi'/\partial\varphi\rangle$ is the angular momentum exchange rate between the waves of surface density and gravitational potential.

Note, that an equation of angular momentum balance obtained from linearized equation (see, e.g. Savonije and Heemskerk, 1990) contains only the first term of the four appearing in the above expression for f, i.e. the one characterizing angular momentum transport due to the Reynolds stress. The second and the third terms describe angular momentum transfer due to (respectively) radial and azimuthal gas flows induced by the nonaxisymmetric wave, and the fourth one arises due to interaction between the perturbations of density and both velocity components. These effects are essentially nonlinear.

4 NUMERICAL RESULTS

Since the results of all the experiments agree qualitatively, we restrict discussion to the run with $\tau_B = 1$, $\varepsilon = 0.3$ and $\lambda = 0.5$.

4.1 Mass Redistribution and Geometry of Perturbations

In all the runs the two stages can be distinguished in the evolution of the gaseous disk.

The first stage lasts for about three typical times of the bar development τ_B. At this stage the gravitational potential wave with amplitude growing in time excites a density wave in the central region of the disk. This wave looks like a barred two-armed spiral wave (see Figure 1). It also grows in time occupying the larger area in r and its pitch angle (the angle between the tangents to the spiral and circumference of a given radius) is $\beta \approx 20 \div 30°$ near the bar edge and decreases along the spiral arm down to zero. When the bar comes to saturation, it no longer supports the spiral wave, and the latter is distorted into the "ring" by differential rotation. Hereafter we use the term "ring" to describe a nonaxisymmetric perturbation looking like a distorted ellipse (dipole and quadrupole components are well recognized), in the same way as it is observed in SB galaxies. This ring-like perturbation, in its turn, moves inwards from dimensionless radius $r \approx 5$ to $r \approx 3$. This is the end of the first stage. At this time the initial radial distribution of the average (over φ) surface density $\langle\sigma\rangle$ suffers significant changes: it becomes lower than the initial value by the factor of 20 in the central region, exceeds it by almost an order of magnitude at $r \leq 0.25$ and decreases by more than an order of magnitude at $1 \leq r \leq 2 \div 3$. Further, this distribution of $\langle\sigma\rangle$ at $r \leq 3$ remains qualitatively same, though the contrasts to the initial value still grow.

At the next stage a quasi-periodic process sets up in the gaseous disk, its quasi-period decreases in time, as well as deviations from periodicity. The quasi-period (QP) is about $T_{QP} \approx 2.5 \div 3$ for the first several QPs, but near the time $t = 14$ its value becomes quasi-steady: $T_{QP} \approx 2$. The sequence of processes during every QP is similar to that described above for the first stage. Visible distinctions are the higher amplitude but smaller linear size of the central bar-like structure and a visible "separation" of the spiral waves from the bar edges† their pitch angles being smaller ($\beta \approx 12 \div 20°$ at the arm beginning) and life time much shorter (during the time of $t \approx 0.5$ the spirals are distorted into a ring by differential rotation) – see Figure 2. In its turn, the ring splits into two rings, the first moving inward to the disk center and the second outward. Though this outer ring motion is essentially supersonic during the first QP's – its starting radial velocity is about $35 \div 45$ at $r \approx 3.5 \div 5$ ($3.5 \div 5$ kpc in dimensional units), it falls to $15 \div 25$ km/s at $r \approx 8$ (and the perturbation vanishes immediately afterward), while $c_s \approx 10$. Naturally, such propagation velocities of the perturbations cause considerable viscous dissipation of energy. In the following QP's the velocities fall to the starting values of about 10 km/s and ending values of about $7 \div 8$ km/s.

The evolution of the surface density Fourier-spectra is shown in Figure 3, the spectra are calculated at four typical radii for six different times during one QP. The symmetry of the computational grid suppresses the odd harmonics and only the even ones appear in the spectra, i.e., $\exp(im\varphi)$ with $m = 2n$, $n = 0, 1, 2 \ldots$

†This effect is due to the density depression in the "background" $\langle\sigma\rangle$. If the contours of the relative amplitude of the perturbations $\sigma/\langle\sigma\rangle$ were plotted, the wave continuity would be evident.

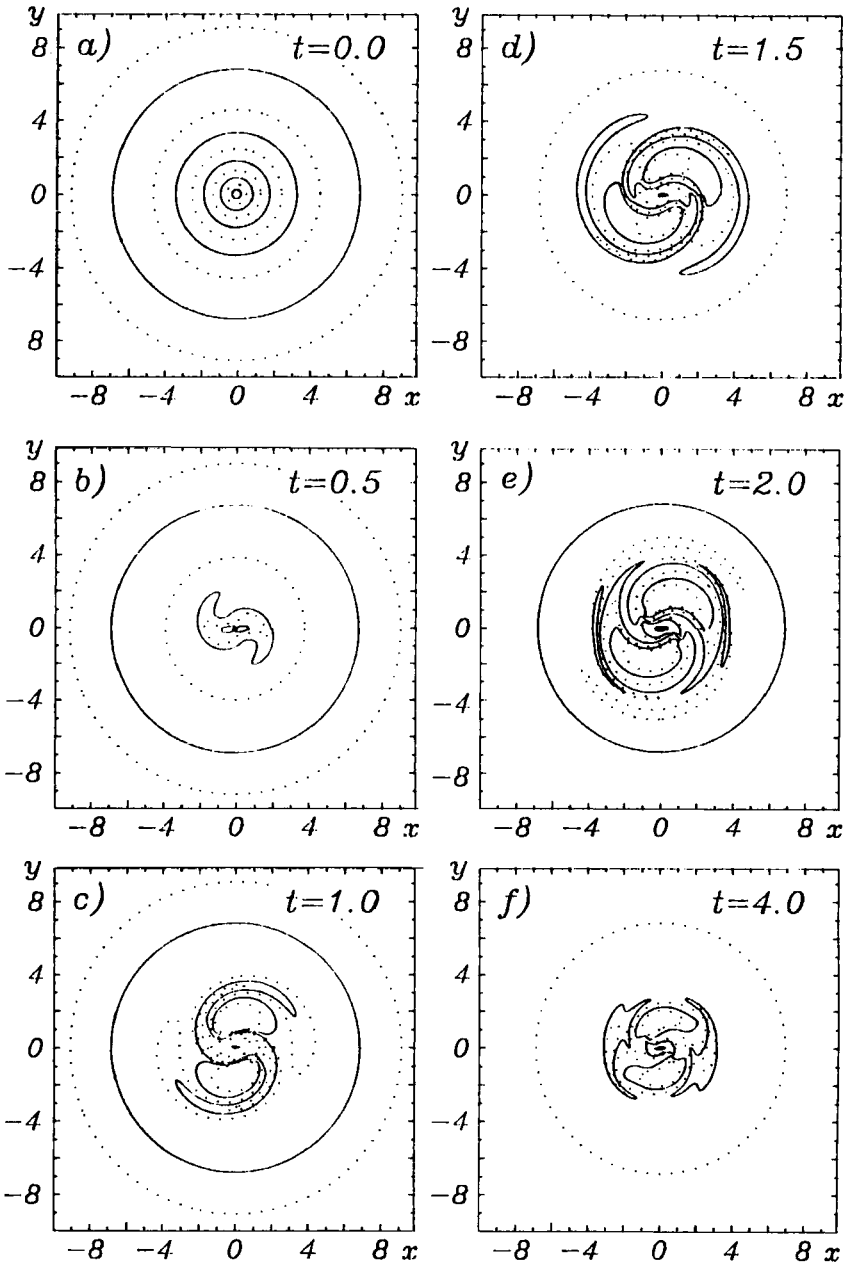

Figure 1 The gas surface density evolution during the first stage. The contour plots are shown for the following levels: with solid lines: *a*, 0.1, 0.3, 0.5, 0.7, 0.9; *b*, 0.1, 0.5, 1.0; *c*, 0.1, 0.5; *d*, 0.01, 0.5; *e*, *f*, 0.001, 0.5; with dotted lines – *a*, 0.05, 0.2, 0.4, 0.6, 0.8; *b*, 0.05, 0.25, 0.75; *c*, 0.05, 0.25, 1.0; *d*, 0.001, 0.1, 1.0; *e*, 0.0001, 0.1, 1.0; *f*, 0.001, 0.5. The closed banana-like contours in Figures 1*c*–*f* depict the regions of minimal density. The bar and gas rotate counter–clockwise.

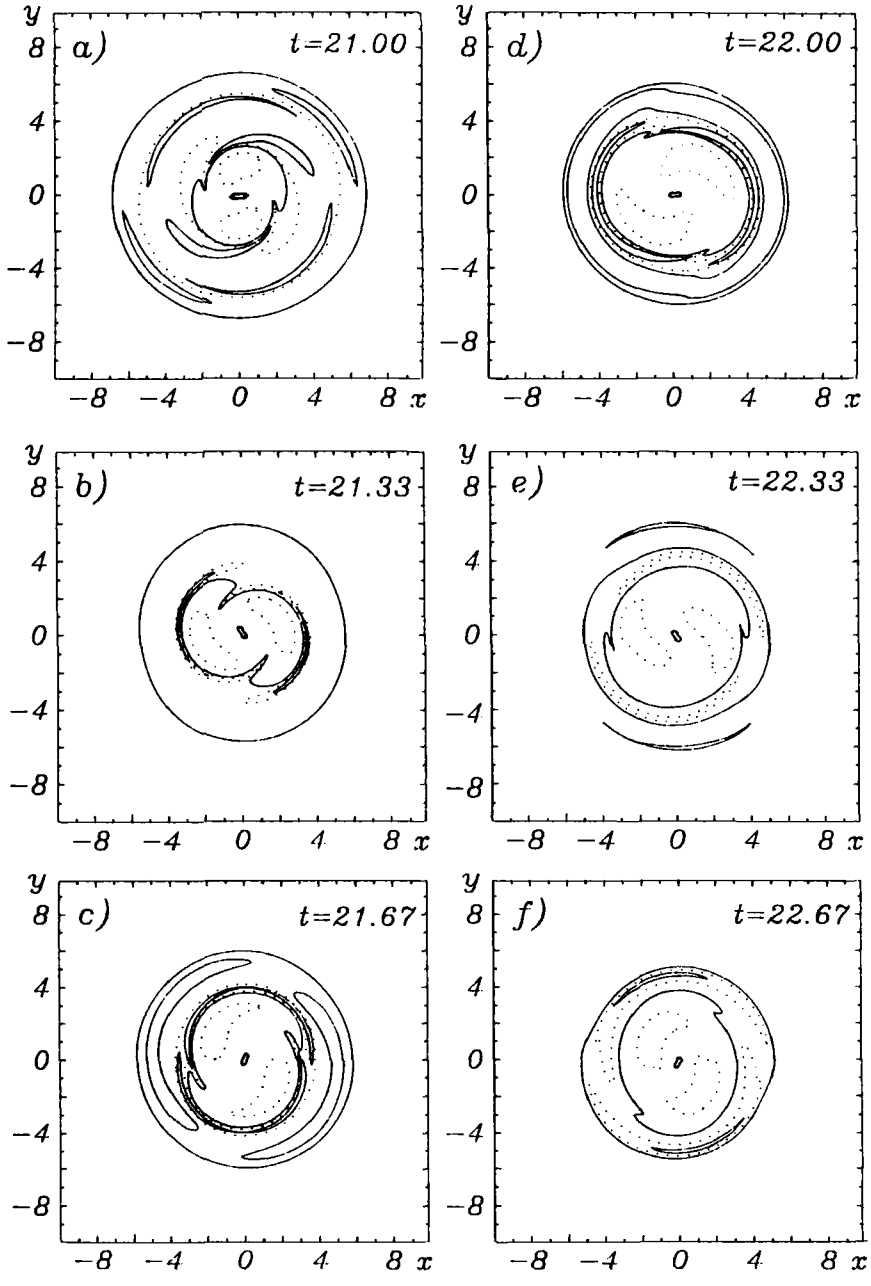

Figure 2 The gas surface density evolution during one of the quasiperiods. The contour plots are shown for the following levels: with solid lines: *a*, 0.1, 0.4; *b*, *c* , 0.1, 0.2; *d*, 0.2, 1.0; *e*, 0.2; *f*, 0.75; with dotted lines – *a*, 0.00001, 0.2, 1.0; *b*, *c*, 0.00001, 0.5, 1.0; *d*, 0.00001, 0.5; *e*, 0.00001, 1.0; *f*, 0.0001, 0.5. The closed banana-like contours in Figures 1*c*–*f* depict the regions of minimal density. The bar and gas rotate counter–clockwise.

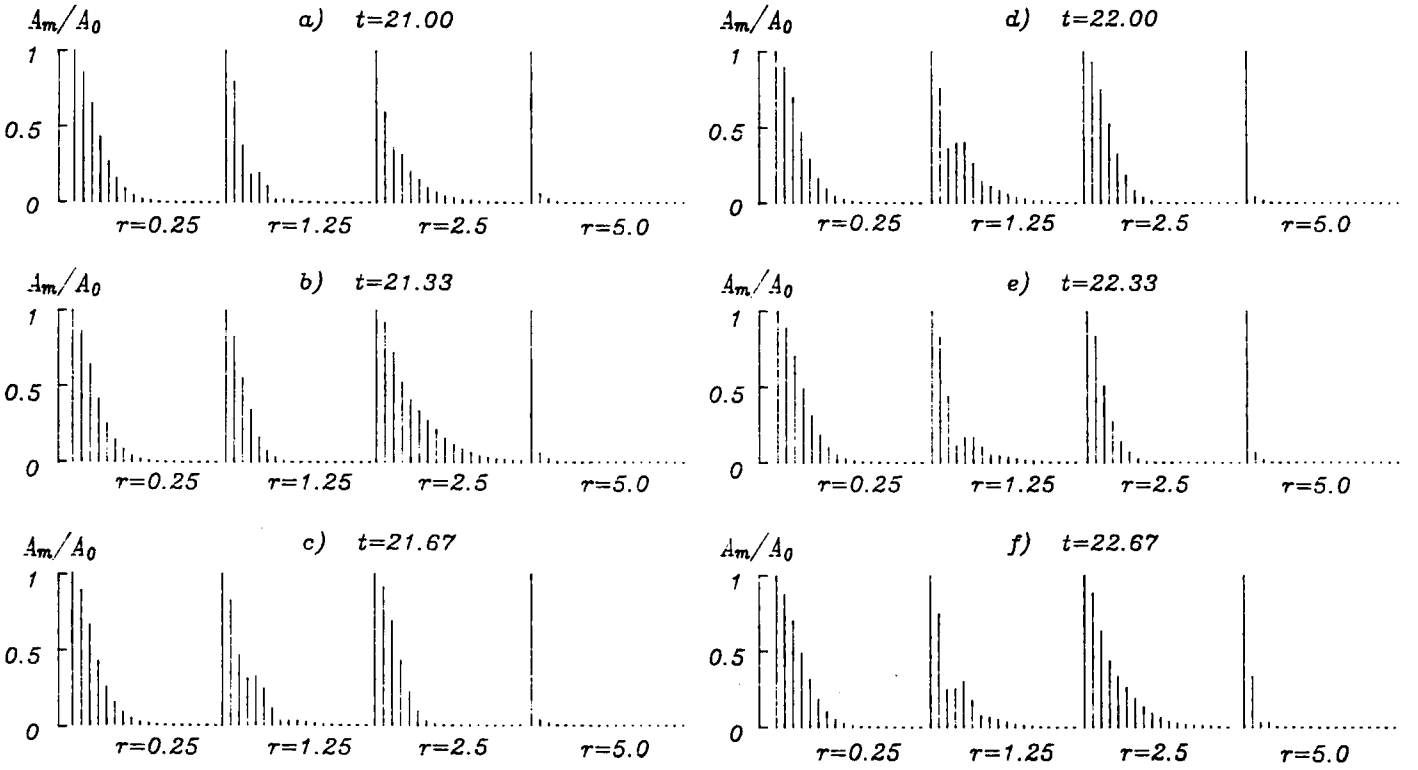

Figure 3 The evolution of surface density Fourier-spectra during one of the quasi-periods for four typical radii. The relative amplitudes are shown for the azimuthal harmonics of $\exp(im\varphi)$ with $m = 0, 2, 4 \ldots$ The highest harmonics shown is the 38th.

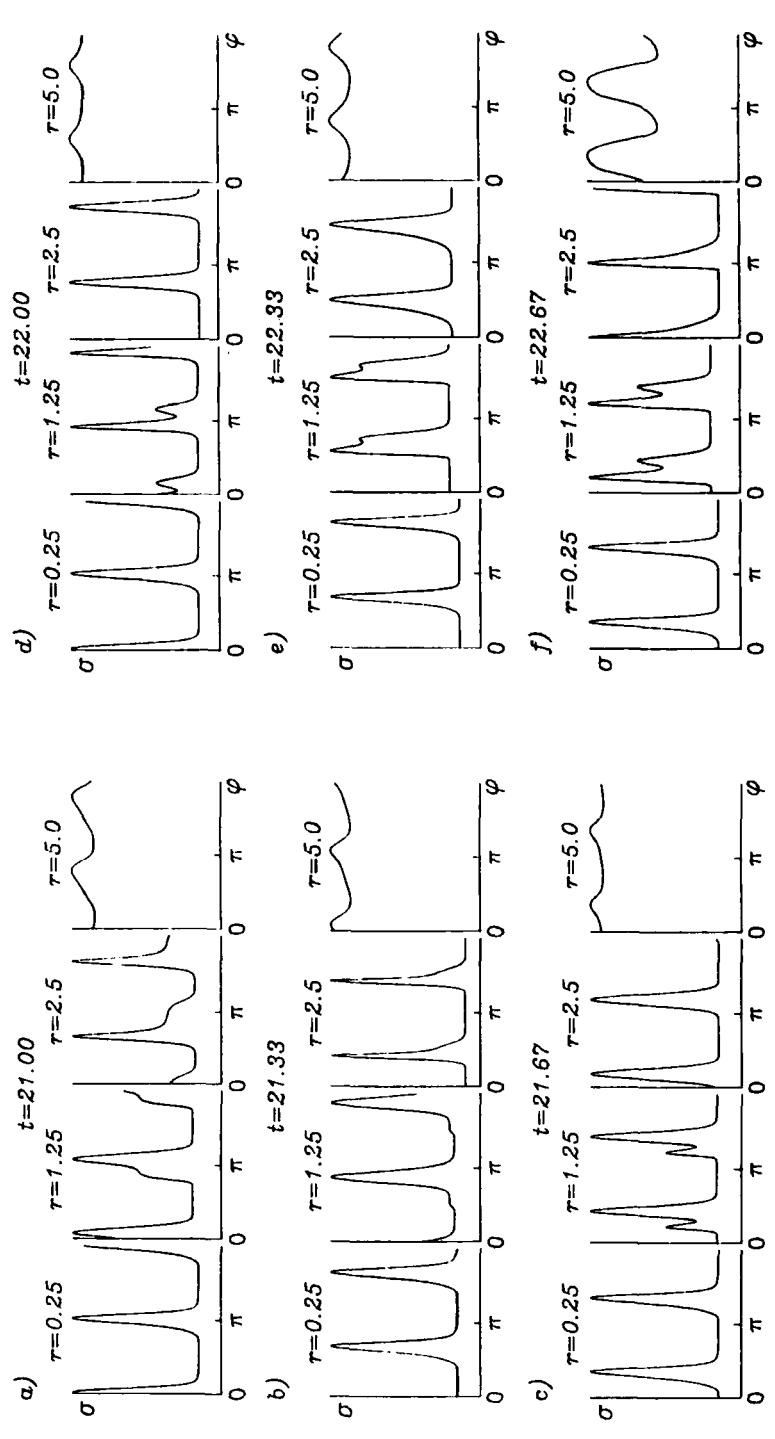

Figure 4 The evolution of the surface density azimuthal profiles during the same quasi-period and at the same radii as in Figure 3. Every panel shows the density normalized to its maximum at a given radius and the time moment.

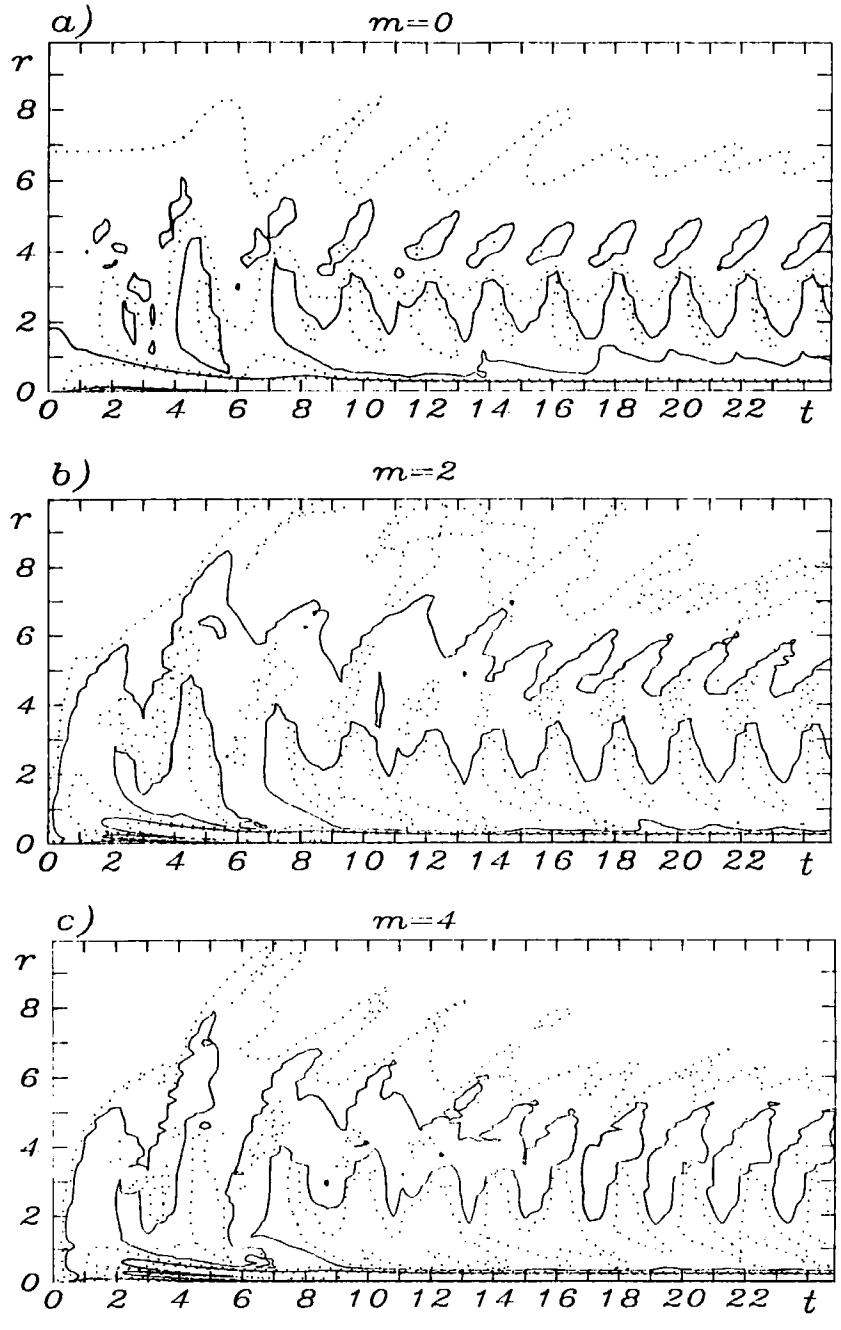

Figure 5 The evolution of amplitudes of surface density predominating azimuthal harmonics $m = 0, 2, 4$. The contours are shown on the plane r, t for the levels 0.001, 0.1, 1.0 (dotted lines) and 0.01, 0.5 (solid lines).

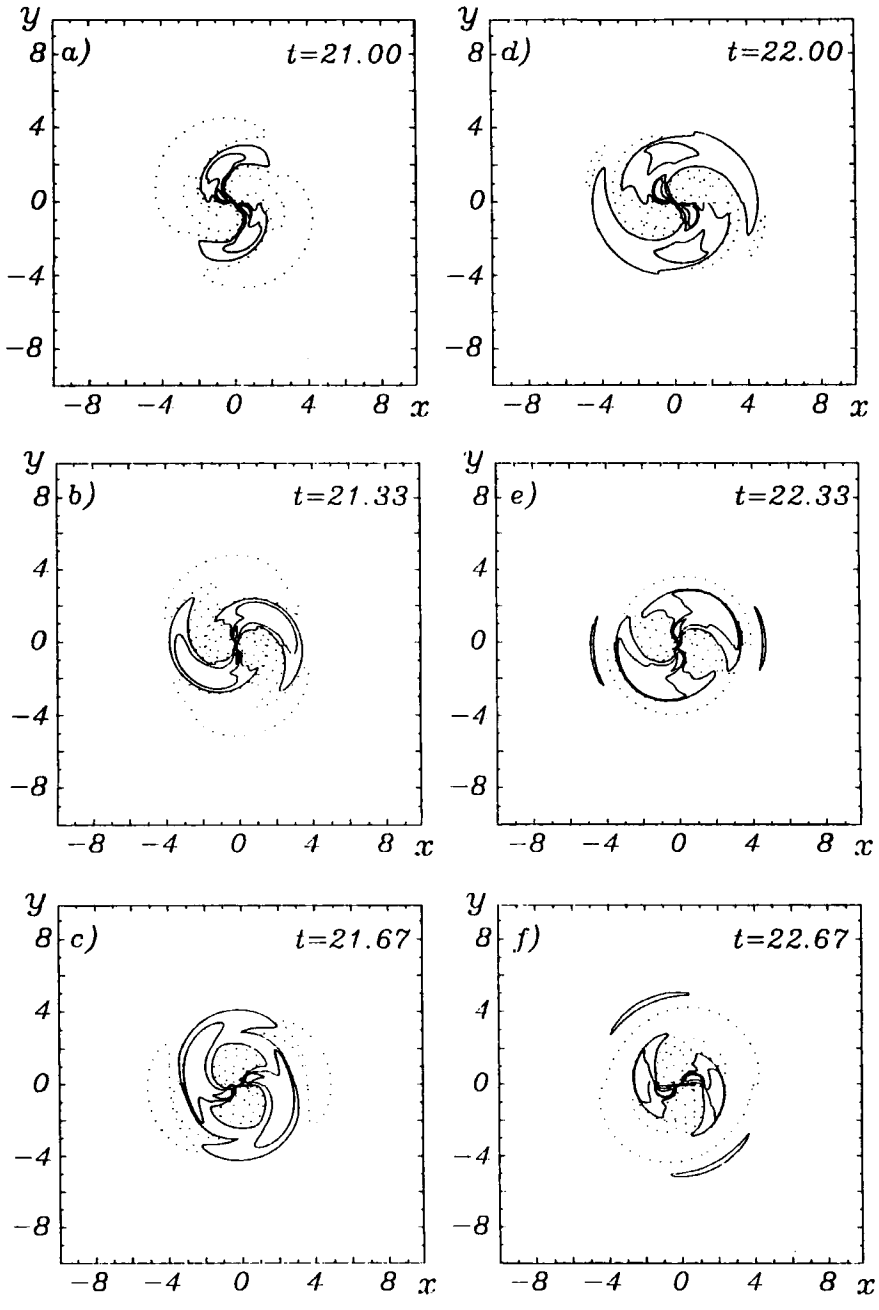

Figure 6 The evolution of the gas radial velocity distribution in the disk plane during one of quasi-periods. Solid lines correspond to the regions where the gas moves outvards, dotted lines– to the center. The levels ±0.1, 0.5, 1.0 are plotted. The bar and gas rotate counter-clockwise. The same moments as in Figures 2–4 are shown.

The corresponding azimuthal profiles of the perturbations are presented in Figure 4.

Figure 5 illustrates the evolution of the amplitudes of dominant harmonics $m = 0, 2, 4$ of the surface density. It shows that all these harmonics propagate outward in the r-coordinate as a sharp peak on the amplitude distribution moving as a whole, while the backward motion rather moves this peak towards lower r's. Thus, the outward motion is a wave propagation, while backward motion is its disruption. The perturbations of the harmonics shown are in phase, which is typical of this process.

The distribution of radial velocities in the disk plane is of certain interest (see Figure 6). Note that our results confirm the results by Afanas'ev *et al.* (1989), who obtained a bisectorial flow structure in similar experiments.

4.2 The Radial Mass Flux

Two regions in the r-coordinate can be distinguished in the gaseous disk where mass transport seems to be quite different.

In the central region (close to the nucleus) the radial mass flux distribution seems to be qualitatively the same during the experiment, the quantitative changes never exceed 50% and occur rather rarely (once per $4 \div 6$ revolutions of the bar). This region radius is maximal ($r \approx 1.8$) at $t \approx 1.5$ and then at $t \approx 4 \div 5$ it falls to the value of $r \approx 0.4$ not changing thereafter. The mean densities of axisymmetric mass flux $\langle\sigma\rangle\langle V_r\rangle$ (Figure 7*a*) and radial mass flux due to nonaxisymmetric perturbations $\langle\sigma' V_r'\rangle$ (Figure 7*c*) are the same by order of magnitude but opposite in direction. The resulting radial mass flux density $\langle\sigma V_r\rangle \equiv \langle\sigma\rangle\langle V_r\rangle + \langle\sigma' V_r'\rangle$ (Figure 7*b*) is co-directed with $\langle\sigma\rangle\langle V_r\rangle$.

In every part of the disk, except the central region described above, the radial fluxes change their direction quasi-periodically in time. The axisymmetric mass flux exceeds the radial mass transport due to nonaxisymmetric perturbations by a factor of $5 \div 10$, but the direction of the flux is always the same, in the contrary to the central region. Though the radial fluxes in this outer region change their direction quasi-periodically, there exist zones where the gas moves only inward or only outward when averaged in time. Figure 7*d* illustrates this fact with contour plots of mass flown through the circumference of radius r from the beginning of the simulation beginning to current time t. This mass is calculated as:

$$dM = \int_0^1 \int_0^{2\pi} \langle\sigma V_r\rangle r \, d\varphi \, dt'. \tag{21}$$

Just as we expected, the mass flux averaged over time and radius is directed to the disk center. The angular momentum transport to the outer regions (see below) and radiation losses cause the gas accretion rate and the system total energy decrease. The total potential energy (defined as integral of $\sigma\psi$ over the disk surface) relative decreasing during the simulation time was $(U_{t=22} - U_{t=0})/U = -0.043$ (here $U_{t=22}$ is the value of U averaged over a QP from $t = 21$ to $t = 23$).

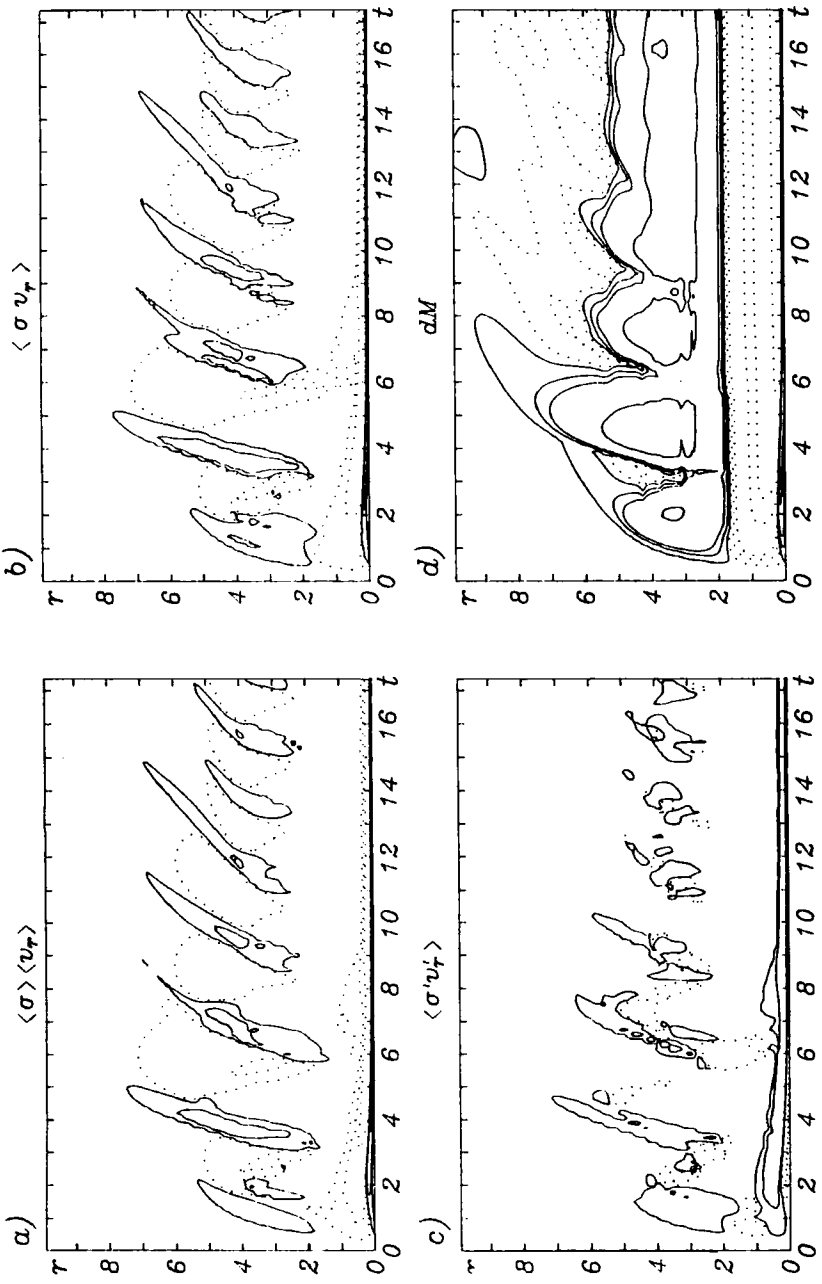

Figure 7 The contour plots of the densities of axisymmetric mass flow (*a*), radial mass transport of nonaxisymmetric perturbations (*c*) and resulting mass flux (*b*). Also the mass flown through the r radius circumference during the time from the simulation beginning till the current time-moment t is shown (*d*). The contour plots for the levels of ±0.01, 0.1, 1.0 (*a*, *b*); ±0.01, 0.1 (*c*); ±0.01, 0.05, 0.1, 0.5, 1.0, 5.0 (*d*) on the plane of (r, t). Solid lines correspond to the mass transport outwards, dotted lines – inwards.

The results exhibit an obvious auto-oscillatory character of the processes occurring in the disk, and since the dissipation is present, an energy source is required. If we assume the stellar bar-mode to be this source, the amplitude of the bar-mode is hardly constant. When the QP process is set, the energy and angular momentum exchange between the bar potential and the gas occurs only at $r \leq 0.5$ (see below). The reason is either the density wave which is almost in phase with the potential wave, so that $\langle \sigma \partial\varphi/\partial\varphi \rangle \to 0$ (cf. Eq. 20), everywhere except the vicinity of the nucleus (see above), or the vanishing amplitude of one or both waves. Thus, gravitational energy released during the gas accretion feeds the auto-oscillatory process.

4.3 Angular Momentum Redistribution

The angular momentum redistribution occurs in different ways in the regions in the r-coordinate with the altering of processes of mass transfer.

In the QP regime the angular momentum flux density distribution along the r-coordinate stays qualitatively the same in the central region. The quantitative changes never exceed 50%, as for the radial mass flux density, the typical times are the same. The radial curves of angular momentum flux density in this region along with the radial distributions of its components (Eq. 20) at $t = 25$ are shown in Figure 8. Comparing Figure 8*e* with 8*f*, one can see that the angular momentum flux of axisymmetric and nonaxisymmetric perturbations compensate each other in the central region. Here the angular momentum density weakly and monotonically decreases with time due to viscous absorption (see Figure 8*g* and 8*h*).

In outer regions all the components of the angular momentum flux are changing in value and direction quasi-periodically. The most intense transport of angular momentum in this region occurs between $r \approx 2.5$ and $r \approx 6 \div 7$, i.e. where the density perturbations of considerable amplitude propagate. Figure 9 illustrates the contributions of different mechanisms into the angular momentum transport by nonaxisymmetric perturbations. One can see that the angular momentum flux density of radial flows induced by nonaxisymmetric waves predominates during all the simulation time. The same follows from the comparison of Figure 10*a* (contour plots of the total mean radial angular momentum flux density of nonaxisymmetric perturbations) and Figure 10*c* (contour plots of its component due to perturbed radial flows). Though the disk is disturbed by the potential wave with the azimuthal wave number $m = 2$, in the region of $2 \leq r \leq 7$ the contributions of axisymmetric flows (Figure 10*b*) and viscosity (Figure 10*d*) dominate in the angular momentum transport. This fact, seeming not so evident, we illustrate in Table 1, where maximal values of different components of the angular momentum flux density in the zone discussed are normalized to the maximal value of the viscous flux[†].

Note that the nonadditivity of intensity maxima of different components of the angular momentum transport by nonaxisymmetric perturbations is due to some lag of these maxima in r and t.

[†]The data in Table 1 correspond to a QP process after it sets.

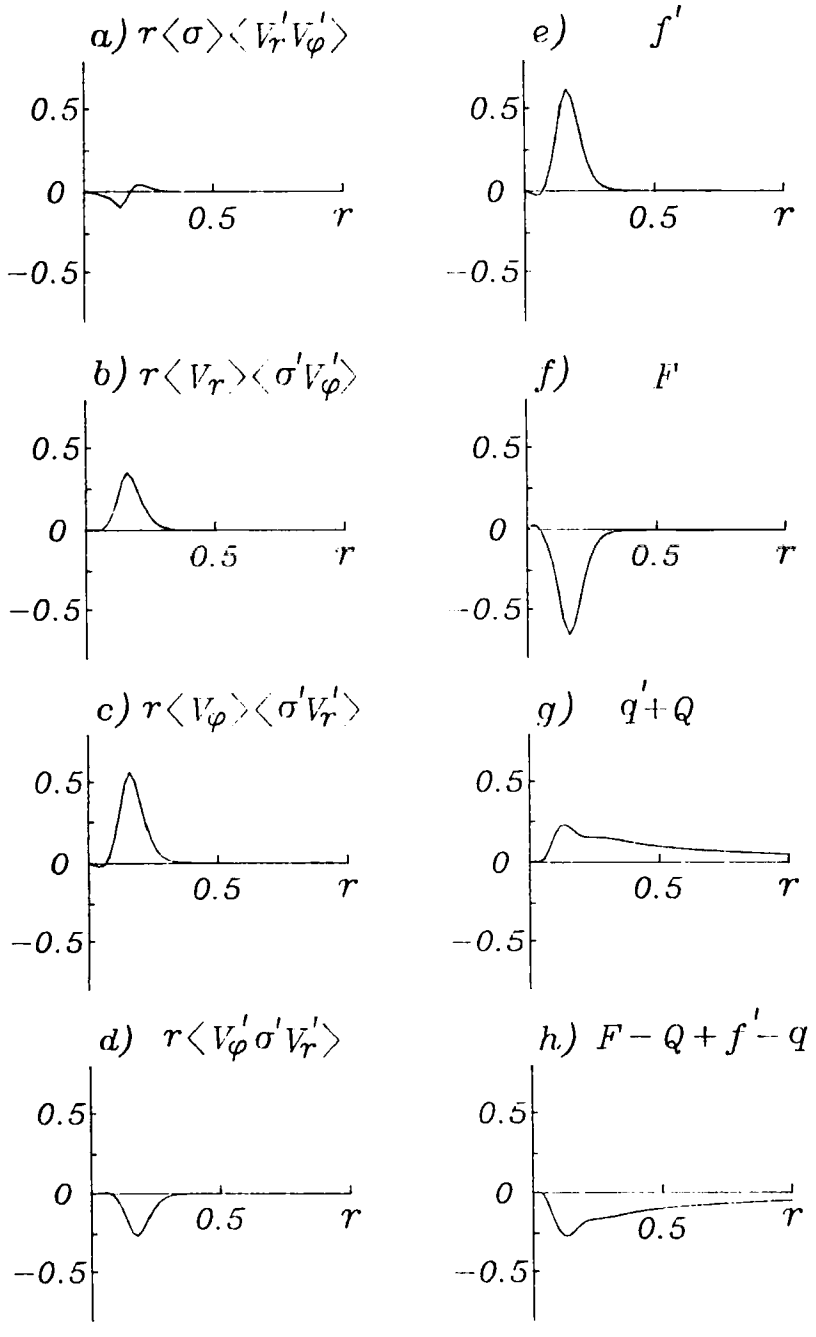

Figure 8 The radial distributions of the mean flux density of the angular momentum and its different components (cf. Eq. 20 and comments there in text) in the central part of the disk for $t = 25$.

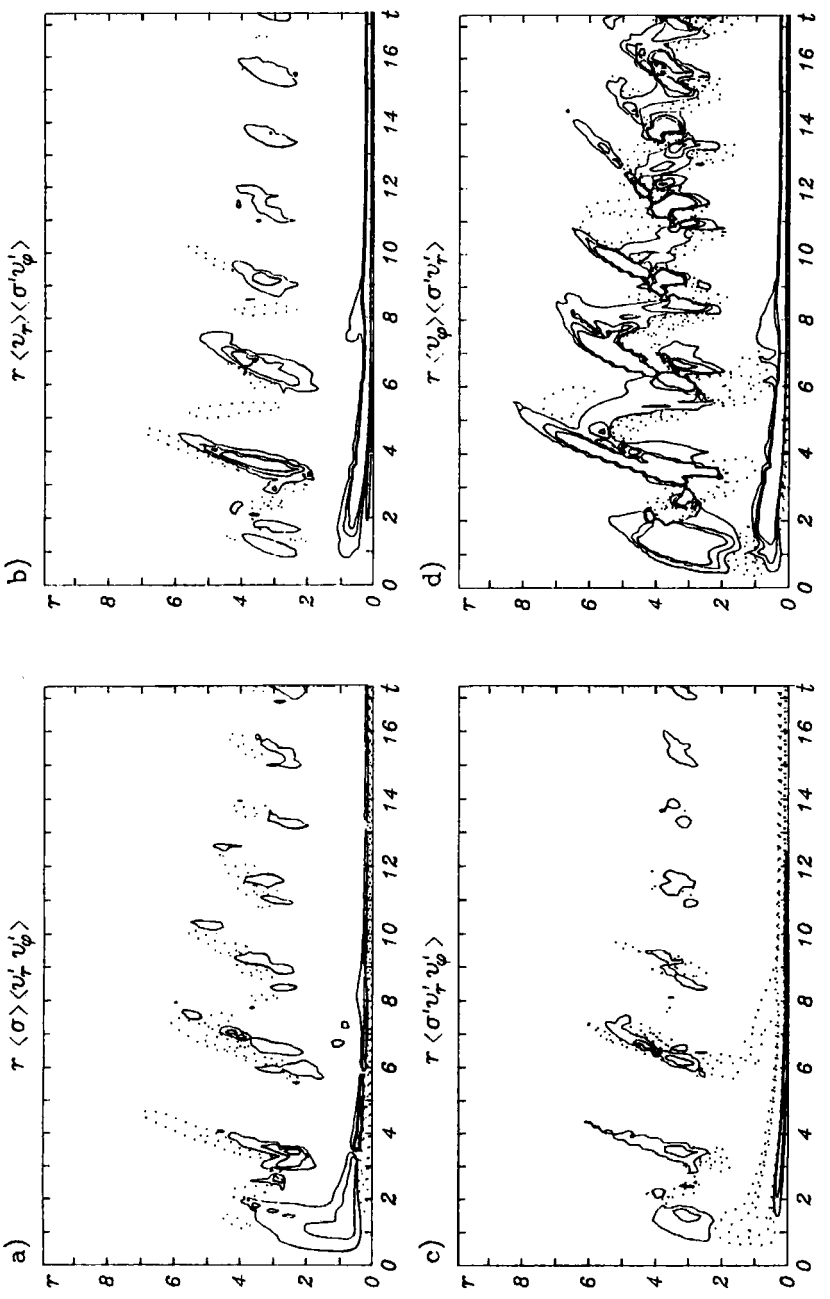

Figure 9 The relative contributions of different mechanisms (cf. Eq. 20 and comments there in text) into the angular momentum transfer by non-axisymmetric perturbations. The contour plots for the levels of ±0.01, 0.05, 0.1 are shown on the plane (r,t). Solid lines correspond to the angular momentum transport outwards, dotted lines – inwards.

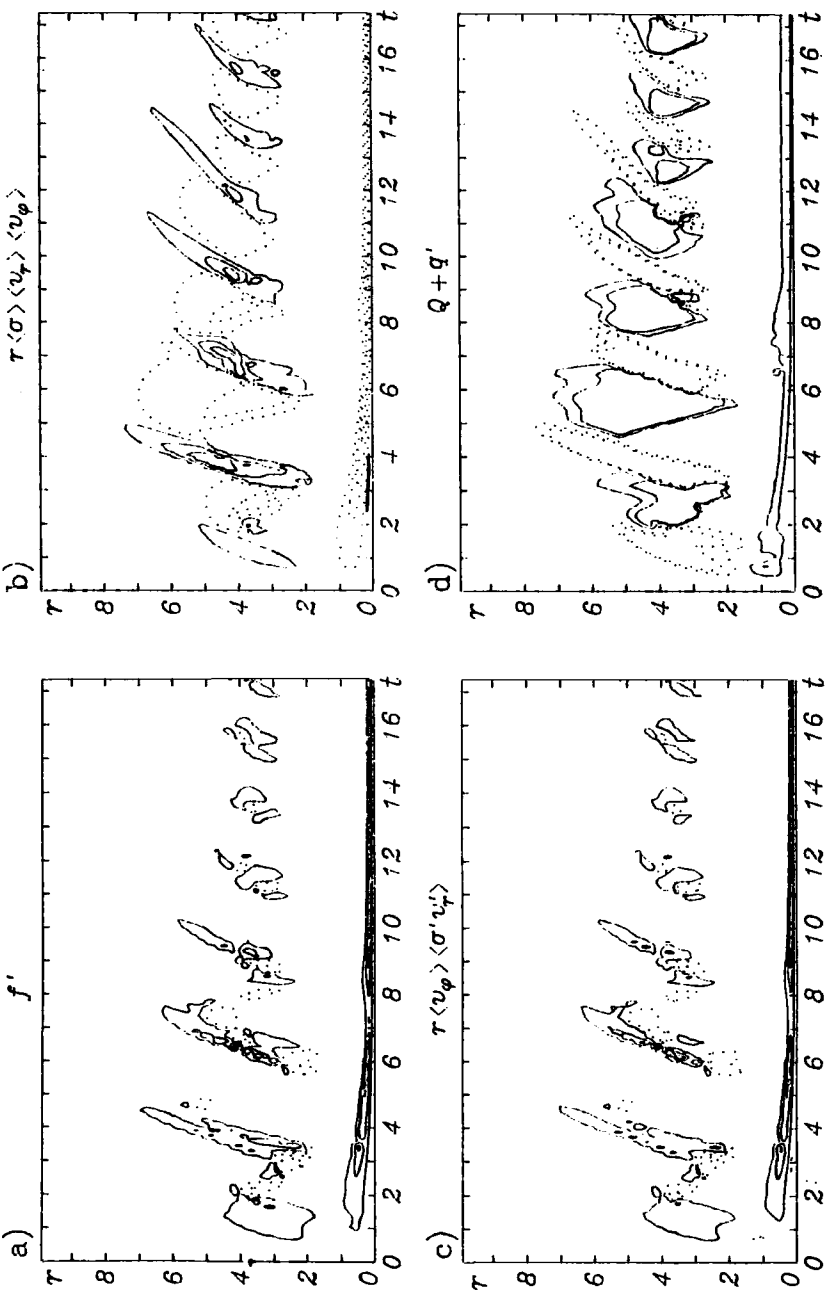

Figure 10 The mean densities of the radial fluxes of angular momentum, transported by nonaxisymmetric perturbations (*a*), by axisymmetric flow (*b*), by perturbed radial flows (*c*) and under the action of viscosity (*d*). The contour plots for the levels of ±0.1, 0.5, 1.0 (*a*, *b*, *c*) and ±0.5, 1.0 (*d*) are shown on the plane (r, t). Solid lines correspond to the angular momentum transport outwards, dotted lines – inwards.

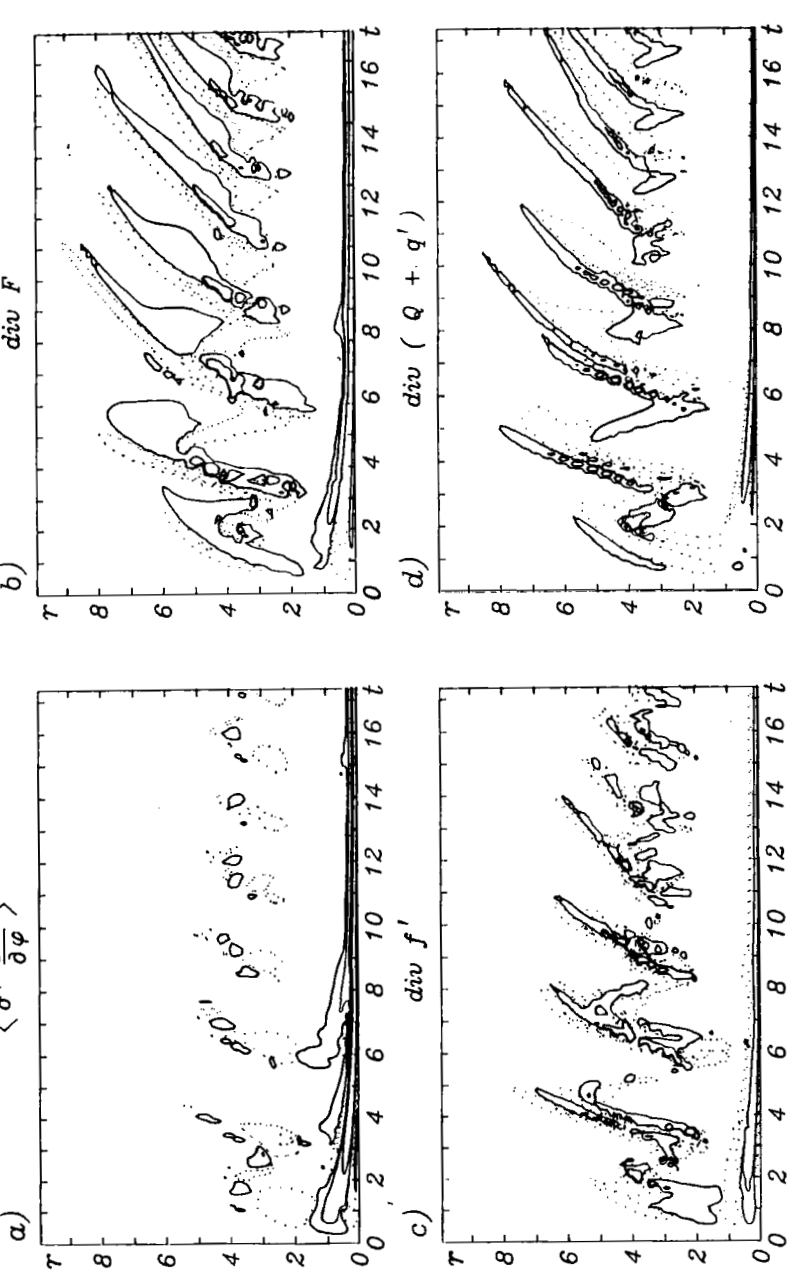

Figure 11 The contribution into the time evolution of the mean density of angular momentum due to gravitational potential wave (*a*), axisymmetric radial flows (*b*), nonaxisymmetric perturbations (*s*) and viscosity (*d*). The contours for the levels of ±0.01, 0.1, 1.0 (*a*); ±0.1, 1.0 (*b*, *c*) and ±1.0, 10.0 (*d*) are shown on the plane (*r*, *t*). Solid lines correspond to negative contours, dotted lines – to positive ones.

Table 1. Maximal relative intensities of the angular momentum flux components

Mechanism of angular momentum transport	*Intensity*
Viscosity	1.0
Axisymmetric radial flows	0.17
Non-axisymmetric perturbations	0.1
Including:	
– perturbation-induced radial flows rotating with basic flow	0.1
– radial drift of induced azimuthal flows in the basic flow	0.02
– Reynolds stresses	0.007
– interaction of V_r^l, V_φ^l and σ^L perturbations	0.007

Rather unexpected is the fact of weak influence of angular momentum exchange between gravitational potential wave and surface density disturbances on the gas angular momentum. Figure 11 shows that, in the QP stage, the rotating potential of the bar very weakly affects the angular momentum outside the central region. In Section 4.2 the reasons for this were discussed: they are a small phase lag between ψ' and σ' at $r \sim 1$ and a small amplitude of ψ' at $r \gg 1$.

4.4 The Physics of the first Stage

The sequence of the processes occurring in the disk may be described in the following way.

The gas flowing across the potential wells of the growing wave of gravitational potential accumulates there. The most rapid accumulation occurs not at $r \simeq 1$, where the well is the deepest (cf. Eq. 6), but at $r \simeq 0.5$ for the following reason. In the central region the kinetic energy of the gas and bar relative motion grows with radius as r^2, and hence, while the well is shallow, this energy together with kinetic energy the gas obtained during its fall into the well may be enough to cross the potential wave, "climbing" up the opposite side of the well. Besides the gas inflow across the direction of the bar's major axis, there exists a radial inflow into the potential well from the innermost region. Since the relative linear velocity of the bar and the rotating gas is small, the gas flows down from potential "humps" towards the central saddle point (cf. Eq. 6) and then into the well.

Non-uniform radial distributions of kinetic energy of the bar and gas relative motion and of the bar potential amplitude change the distribution of the phase lag between the potential waves and the density wave localized in it. Inside of $r \simeq 1$ (the constant angular velocity region) the lag is constant with radius, the potential minimum following the surface density maximum (in the gas rotation direction). With r growing from $r \simeq 1$ to $r \simeq 1.3$ this phase lag steeply grows, and, beyond $r \simeq 1.3$, falls rather rapidly, and the density wave appears to be a trailing spiral with a rather small pitch angle (cf. Section 4.1). The density maximum typically coincides in φ-coordinate with potential minimum at $r \simeq 1.9$, i.e. at the corotation radius r_c of the bar potential wave and the density wave localized in it. These results agree well with those of Roberts (1969), Baker and Barker (1974) and Kovalenko

and Levy (1992), where it was shown that the shock wave develops on the rear (with respect to the gas flow) side of the potential well, then moves upstream to the front side, and is finally placed there if the inflow is steady. In our simulation, while the potential perturbation increases, the wave maximum slowly moves from the rear to the front side of the well and stops there at the end of the first stage. It is implied by the distribution of the phase lag between σ' and ψ' that the gravitational potential perturbation extracts the angular momentum from the density wave inside r_c and vice versa (cf. Eq. 20). The phase lag is such that $r\langle\sigma' V_r'\rangle < 0$ at $r < r_c$ and $r\langle\sigma' V_r'\rangle > 0$ at $r > r_c$, therefore the wave angular momentum grows in time (in absolute value), and the wave is amplified while the bar amplitude is increasing.

In our simulation the linear stage of perturbation evolution is very short – soon after the bar is "switched on", the higher harmonics of short wavelengths appear in the perturbation spectrum, and in the central region the perturbation seems to create the shock wave. Afterwards, the shock waves play an important role in the dissipation and nonlinear interaction between the mean flow and perturbations. Inside the corotation radius the mean flow leaves the wave behind and feeds it with energy and angular momentum; at $r > r_c$ the wave runs ahead of the gas mean flow and, hence, speeds it up transferring to it the part of its energy and angular momentum. The angular momentum flux of nonaxisymmetric perturbations is directed outward from r_c. Since at $r < r_c$ the wave angular momentum is negative, the wave transfers the angular momentum from inner to outer regions. The process described and the efficient dissipation of nonlinear short wavelength harmonics provides a part of the transport of the angular momentum of the axisymmetric flow from the region $r < r_c$ to $r > r_c$. A similar process occurs during the wave self-amplification due to resonant instabilities in the gaseous disk (see, e.g., Savonije and Heemskerk, 1990; Papaloizou and Savonije, 1991), but its typical time scale is greater by a factor of $10^2 \div 10^4$ and, consequently, the angular momentum transfer rate is much lower.

The viscous transport of angular momentum is much more intense, and it is directed away from r_c. The explanation is that (first) the rotation curve has an inflection point somewhere around this radius and (second) the negative angular momentum dissipates in higher harmonics inside r_c, while it is positive outside r_c.

The angular momentum redistribution by viscosity and waves produces a radial axisymmetric gas flows from r_c. At $r > r_c$ the gas which obtained energy excessive for its orbit moves outwards, while at $r < r_c$ the gas that lost some angular momentum falls to the center. It seems to be significant that accreting gas gains velocity with respect to that of its previous orbit. This resembles a well-known virial effect, but modified by continuity and compressibility of the medium: a fluid particle moving *inertially* passes through the equilibrium orbit corresponding to its new angular momentum value and stops at a smaller radius, it cannot, though, return to the equilibrium epicycle for other particles, having lost their angular momentum for the same reasons. The particle rotation velocity exceeds the equilibrium value for a given orbit since the angular momentum tends to be conserved.

Thus, when the bar comes to saturation, the rotation velocity in the central region grows with respect to the equilibrium value, the excess of centrifugal force

in the radial balance being compensated by pressure gradient and viscous force. A surface density, pressure and angular momentum depression is formed near the corotation radius. Outside the hollow, the gas gains radial momentum and moves outwards as a density wave with a steep front, significant amplitude and supersonic velocity.

Since then the disk is divided into two parts almost independent from each other dynamically. The material deficit in the density hollow region does not allow the density wave to gain significant amplitude near r_c, so the angular momentum exchange between the bar and the gas ceases at $r > r_c$ (Eq. 20). Thereafter the bar potential role is restricted to supporting the existing bisectorial flow structure, the density depression at the center and the density minimum at $r_{\rm ILR} < r < r_{\rm OLR}$ (OLR and ILR are Lindblad resonances, the outer and the inner). Therefore we restrict our discussion to gas dynamics at $r > r_c$.

The perturbation moving outwards at a supersonic velocity quickly looses its energy in dissipation. A significant positive pressure gradient and still growing uncompensated gravitational force (due to a decrease in the rotation velocity of fluid particles moving outwards and their tendency to conserve angular momentum) enhance this process. The wave stops as a result, and the density peak produced by the wave forces it to spread inwards. Simultaneously the angular momentum flux density becomes negative, since its component $F = r\langle\sigma\rangle\langle V_r\rangle\langle V_\varphi\rangle$ becomes dominant (the perturbation is ring-like at that time due to differential rotation). This backward motion makes the previous steep profile flatter, so the viscous effects become weaker and, hence, as the accreting gas angular momentum is conserved to a great deal, it gains rotation velocity moving inwards. It may locally exceed the value $V_\varphi(t = 0)$ because some angular momentum was transferred to this gas in the previous phase of the first stage. Nevertheless, that does not occur while $\langle V_r\rangle$ is not small.

The situation changes when the gas moving inwards approaches the OLR from which the perturbations may be reflected (see, e.g., Savonije and Heemskerk, 1990; Papaloizou and Savonije, 1991). Here the gas (and its angular momentum) is accumulated for some period of time. It results in the appearance of a local region, where the specific angular momentum decreases outwards at $r \approx r_{\rm OLR}$, and the square of epicyclic frequency falls below zero: $\kappa^2 = 2\langle\Omega\rangle(2\langle\Omega\rangle + rd\langle\Omega\rangle/dr) < 0$.

4.5 The Physical Origin of the Quasi-Periodicity

Before the beginning of every QP a region (in r-axis) is formed in the dick where $\kappa^2 < 0$ (see Figure 12*b*). Such a distribution of rotation velocity corresponding to specific angular momentum $\langle\Omega\rangle r$ decreasing outwards is known to be centrifugally unstable, even if the radial forces are balanced (cf. Eq. 9) – see Morozov (1977, 1979, 1989), Fridman (1990) and Baev (1989). In our case the rotation curve in this region goes above the equilibrium one (cf. Figure 13*a*, *b*), which leads to the "explosive" development of the centrifugal instability. An interesting fact is the appearance (as a result of this) of a wave with the symmetry index (a nonlinear analog of the azimuthal mode number m) *is* = 2 along with an axisymmetric perturbation with

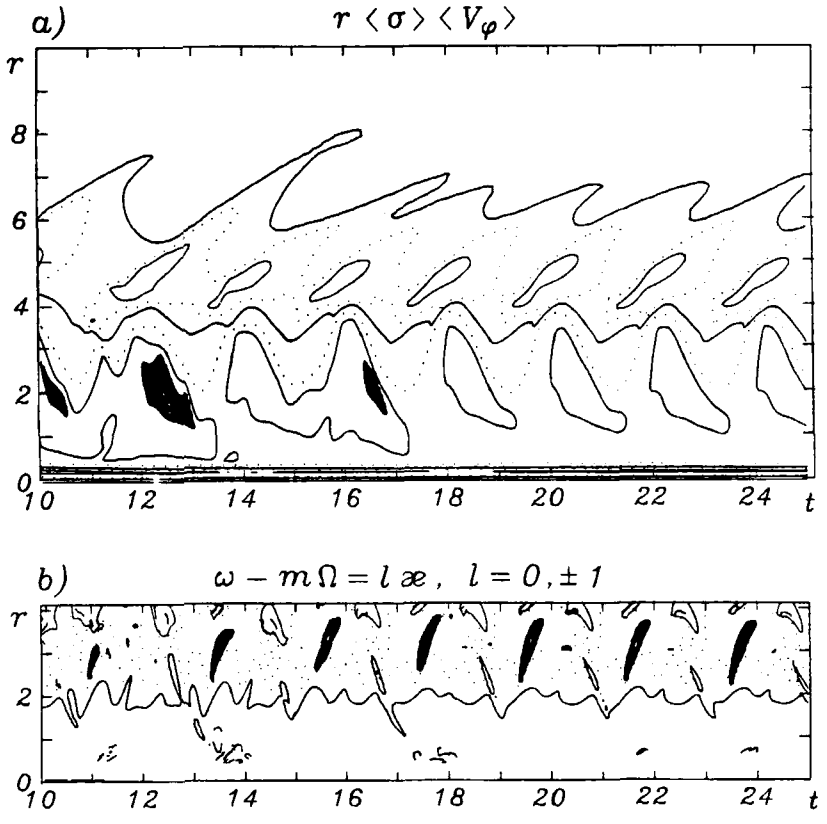

Figure 12 The evolution of the mean density of the basic flow angular momentum (*a*) and of dynamic resonances and the position of regions in the r-axis where the specific angular momentum decreases outwards ($\kappa^2 < 0$) (*b*) on the plane (r, t). In Figure 12*a* the contours for the levels of ± 0.1, 2.0 (dotted lines) and ± 0.01, 1.0, 4.0 (solid lines) are shown; the areas inside of the contour 0.001 are dashed. In Figure 12*b* solid lines correspond to the corotation radius, dotted ones – to the OLR. The regions of $\kappa^2 < 0$ are shown dashed.

$is = 0$. A superposition of both produces rather complicated perturbed density patterns, as it was predicted by Morozov *et al.* (1992) from the linear analysis basis.

The system supporting centrifugal instability evolves to equilibrium (according to the Le Chatelier principle), i.e. the region of $\kappa^2 < 0$ tends to vanish†. This process cannot occur through transport of angular momentum inwards, because the excess of it would increase there. The angular momentum is transported outwards via $is = 2$ and $is = 0$ waves (the latter case is obvious, for the material with its angular momentum is thrown out by uncompensated centrifugal force). Meanwhile, some part of the gas still moves inwards from the outer (with respect to the $\kappa^2 < 0$

†Baev (1989) showed similar process in a disk without bar but with a rotation curve with velocity kink.

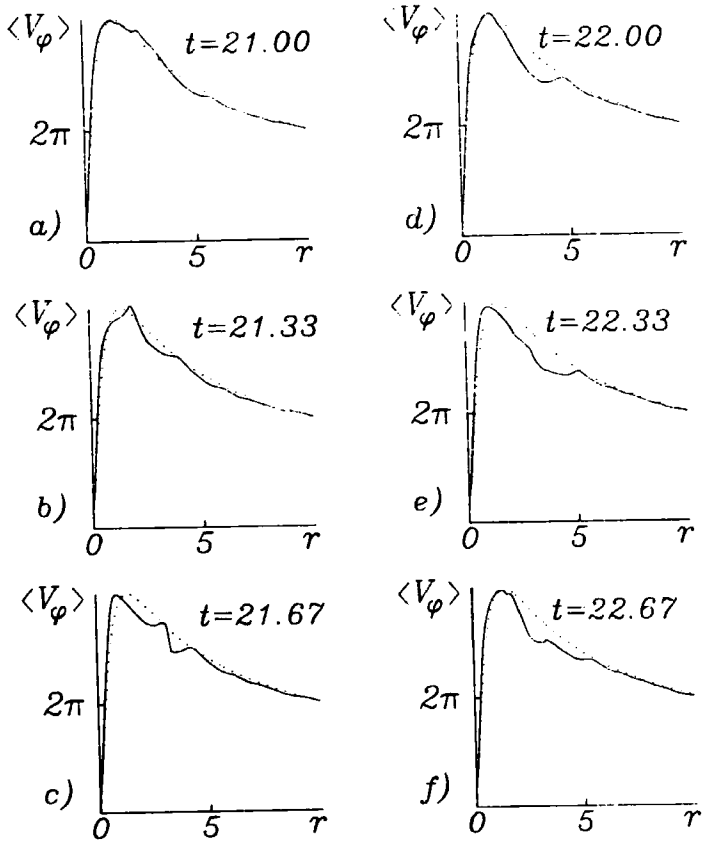

Figure 13 The evolution of the gas rotation curve during one of the quasiperiods. The dotted line showes the initial (at the time of $t = 0$) rotation curve. The time moments are the same as in Figures 2–4, 6.

region) disk (this motion starts much earlier – in the previous QP or at initial stage), so oppositevely directed angular momentum fluxes arise, and hence the region of $\kappa^2 < 0$ survives for some time moving outwards (see Figure 12*b*).

Comparing Figures 12*a* and 12*b* one can see that the radial flux changes its direction somewhat earlier than the $\kappa^2 < 0$ regions appear. So the twoarmed spiral pattern does. The reasons are the following:

(1) before the $\kappa^2 < 0$ regions appear, the Kelvin–Helmholtz instability mechanism (the Bernoulli effect) excites the longest wavelength perturbation ($is = 2$). It can reveal itself even if the rotation velocity falls slower than $\Omega(r) \propto r^{-2}$ (Morozov *et al.*, 1985*b*);

(2) the spiral waves grow faster then Morozov *et al.* (1985*b*) predicted, because initial perturbations of $is = 2$ are of finite amplitude – "rigid" excitation.

(3) the latter makes the nonaxial symmetry to be essential, hence, two local in φ diametrical areas of $\kappa^2 < 0$ appear before the region of $\kappa^2 < 0$ from $\langle V_\varphi \rangle$ forms.

(4) the centrifugal mechanism amplifies the existing spiral wave and its pitch angle decreases.

After the angular momentum flux directed outwards is established, the disk evolution is similar to that in the corresponding periods of the first stage.

We should note that a quasi-periodic process of the same nature for $is = 0$ perturbations occurs in the laboratory experiments simulating the centrifugal instability in a rotating set-up with "shallow water" – cf. Morozov *et al.* (1984, 1985a) and Nezlin and Snezhkin (1990)†. When the mode $is = 0$ was developed, the fluid moved outwards from the velocity jump zone and the instability stopped. When the wave reflected from the set-up outer boundary returned, the instability arose again and so on. Our results allow to suppose that such a regime (called the relaxation regime by Nezlin and Snezhkin, 1990) can occur with no reflection from outer boundaries, due to retiring by pressure gradient, and, surely, due to non-compensated gravitational force, growing while the fluid (tending to conserve the angular momentum) moves outwards.

Also one can notice that in our simulation as well as in the experiments of Morozov *et al.* (1984, 1985a, 1985c), Baev (1989) and Nezlin and Snezhkin (1990) when centrifugal instability drives spiral waves, banana-like anti-cyclonic vortices appear between the arms, localized around the minima of two-dimensional distribution of surface density. See Nezlin and Snezhkin (1990) for detailed description of the vortices and their origin.

4.6 Regions of Radiation and Possible Complex Formation

Though our model is somewhat simplified and is not self-consistent, we think it to be useful to discuss the results that may be compared to the observational data.

The evolution of regions where the dispersion of velocities of cloudmolecules exceeds the value corresponding to $e_{\max}$ (i.e. to temperature $T \simeq 10^4$ K) during one quasi-period is shown in Figure 14. In these regions intense radiation from the (common) inter-cloud gas should be observed as it was discussed in Section 2.2.

If parameters of the gas of cloud-molecules are known we can estimate the areas of possible giant molecular clouds formation (Goldreich and Tremaine, 1982) in accordance with the scenario of GMC formation due to gravitational instability proposed by Gorbatski and Usovich (1986). Figure 15 shows the regions of small Jeans scale (in two-dimensional geometry it is defined as $\lambda_J = c_s^2/(G\sigma)$ – cf. Toomre

†In these experiments, velocity jump on the equilibrium rotation curve led to the centrifugal instability. The gravitational potential distribution simulated with the bottom shape was axisymmetric.

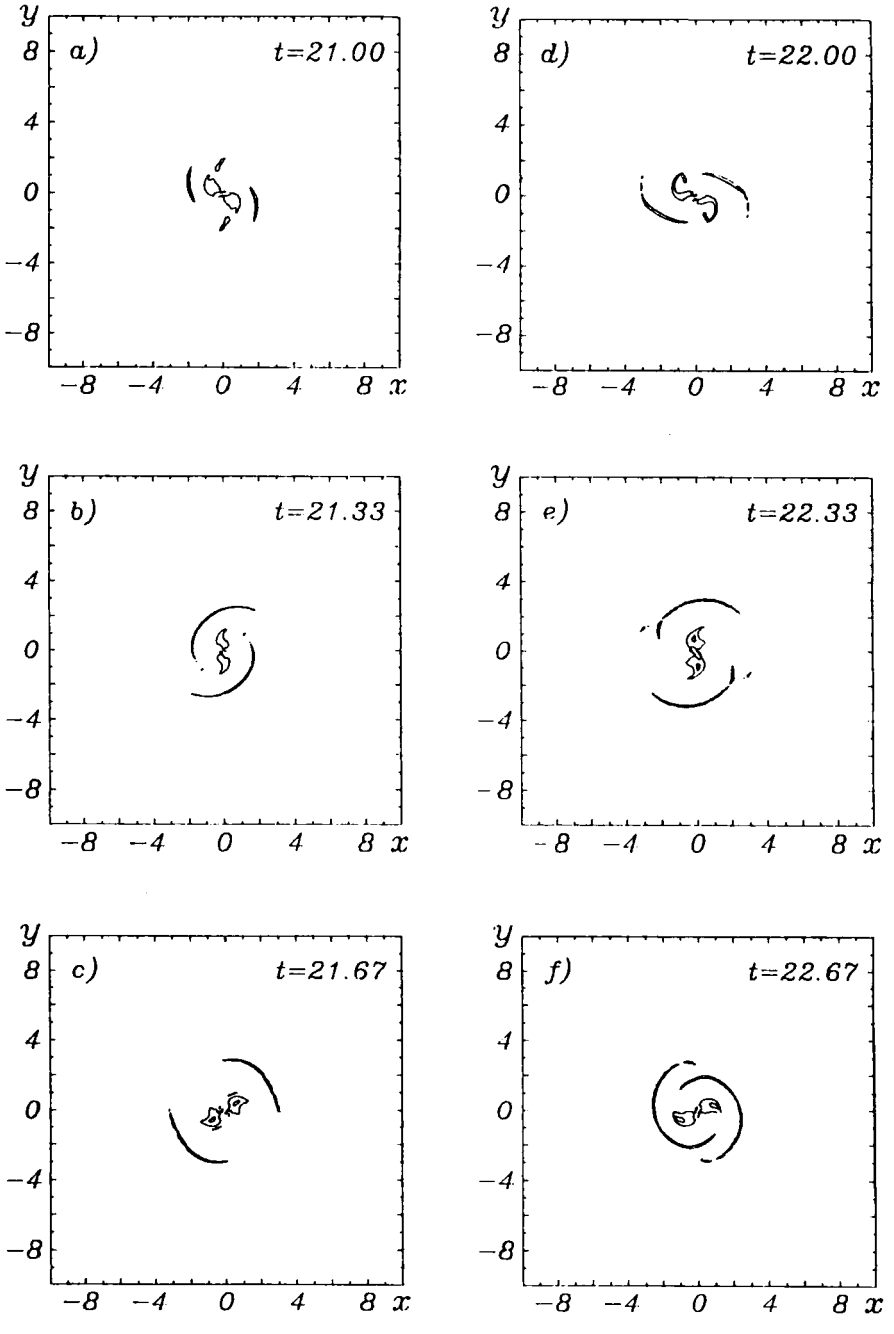

Figure 14 The evolution of the regions in which the gas is radiating (contoured) during one of the quasi-periods. The bar and gas rotate counter-clockwise. The time moments are the same as in Figures 2–4, 6, 13.

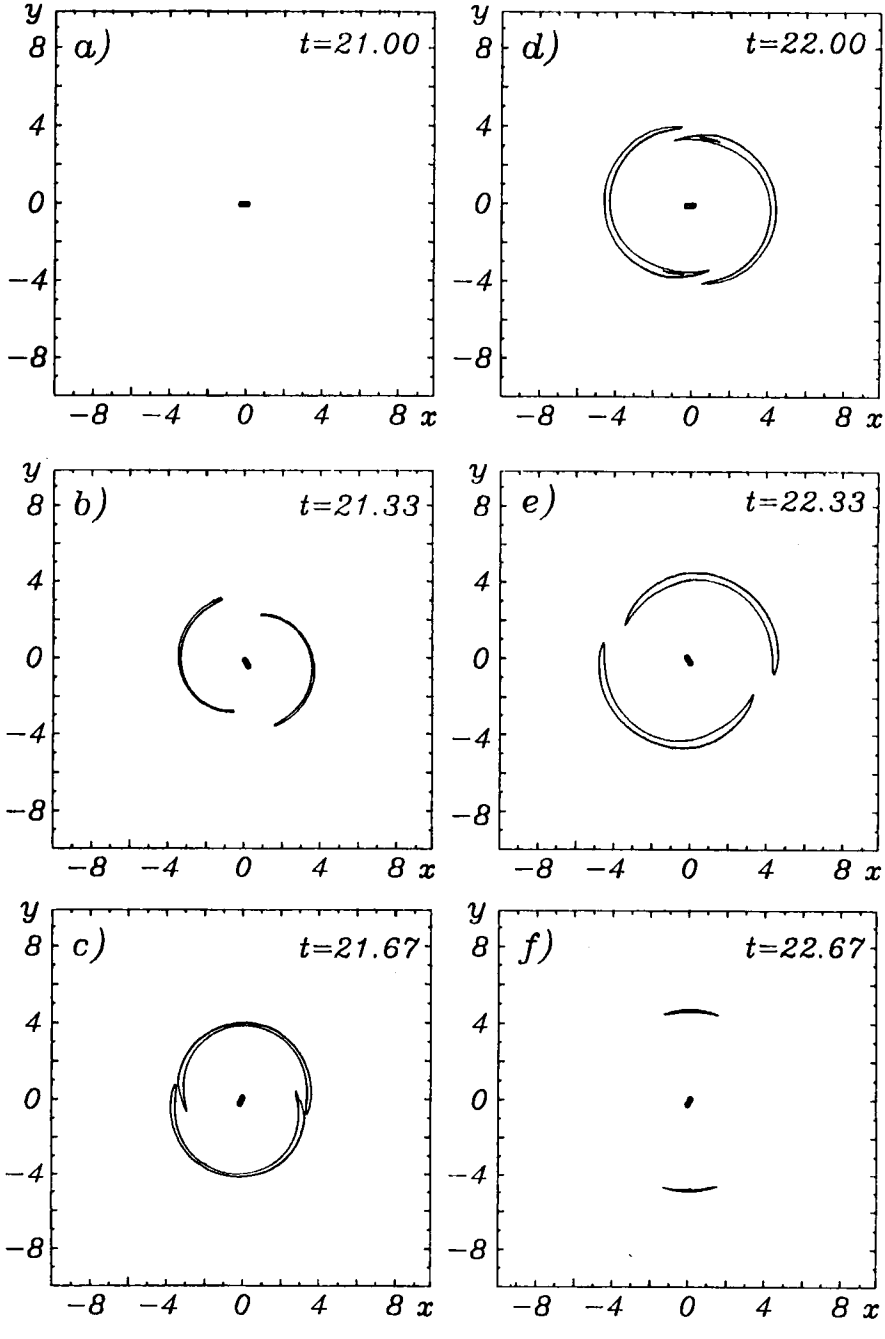

Figure 15 The evolution of the regions in which the Jeans scale is smaller than 50 pc (contoured) during one of the quasi-periods. The bar and gas rotate counter-clockwise. The time moments are the same as in Figures 2–4, 6, 13, 14.

1964[†]) where the GMC formation may be expected. Note that in the regions shown in Figure 15 λ_J falls down to $30 \div 50$ pc, i.e. becomes of the order of the size of GMC observed in the Galaxy – Golreich and Tremaine (1982). Since the possibility of GMC formation in frames of such a scenario is discussed by Usovich (1988) (all necessary estimations are given there), we restrict ourselves to pointing out the fact that the quasi-periodic displacement of the regions considered in r and φ coordinates and the cloud gas flows through the regions may lead to molecular ring formation in vicinity of $2 \lesssim r \lesssim 5$ kpc just like in the models Gorbatski and Serbin (1983), Gorbatski and Usovich (1986), Usovich (1988) considered. Note that GMC formation must occur somewhat faster than it was expected from Usovich's (1988) estimations because the instability is not purely gravitational but rapidly dissipative one (Morozov *et al.*, 1986). The viscosity diminishes the intensity of chaotic thermal motions of the clouds which surely is not of help for the GMC formation.

Such small values of λ_J stress that account of self-gravity is needed. We plan to include this and some other factors in the following series of simulation.

4.7 Simulations with other Values of Parameters

Some general considerations allow us to assume the existence of threshold values of the bar amplitude growth rate and its rotation velocity that are crucial for the QPR.

Suppose that the bar linear velocity with respect to the gas in the disk's central part is subsonic: $r(\Omega(r \lesssim a) - \Omega_B)/c_s < 1$. Hence, the shock waves will not appear in the potential well of the bar and, therefore, the density perturbations going from the bar ends will be small. So, the angular momentum transport in the outer regions of the disk will depend on viscosity to a great deal, and the disk evolution, in general, will occur in a way simulated by Gorbatski and Serbin (1983) and Gorbatski and Usovich (1986).

A similar situation occurs when the gas and bar relative velocities are large. Afanas'ev *et al.* (1989) showed that shock waves never appear in experiments with a retrograde bar, for the gas kinetic energy is large enough to allow the gas to cross the potential well of the bar. Besides, the larger the gas and bar relative velocity is, the larger corotation radius and OLR are. But the QPR described above requires rather long (in radius) area between the OLR and the disk edge. The wave going outwards can be reflected by the potential gradient (due to a rather sharp edge of the stellar disk) in a more realistic model.

Unfortunately, we could not simulate significant shift of the corotation radius outwards in our series of experiments because a non-physical reflection at the grid edge is inevitable. Small shifts of the corotation radius (from $r \simeq 2$ to $r \simeq 3$ corresponding to $\Omega_B \simeq 88$ km s^{-1} kpc^{-1}) does not lead to qualitative differences.

[†]We do not use the Toomre–Goldreich– Lynden–Bell criterion (Toomre, 1964; Goldreich and Lynden–Bell, 1965) and the unstable wavelength range determined from it, since the regions of $\kappa^2 < 0$ periodically appear in our simulations.

It seems to be natural that initial radial momentum obtained by matter in the first stage (up to the moment when the spiral perturbation is distorted into a ring-like structure) depends primarily on the bar amplitude growth rate. Nevertheless, when we changed its typical growth time from $\tau_b = 1$ to $\tau_B = 3$ we observed no significant difference, even the first stage time-scale remained the same. The point is that, though the force driving matter outwards is smaller, it acts for longer time, and the momentum becomes smaller only insignificantly. Yet this effect occurs, the evidence is the smaller value of the maximal radius which the perturbations reach during the first stage. It falls from $r_{\max} \simeq 5.7 \div 6.0$ in the model with $\tau_B = 1$ to $r_{\max} \simeq 4.8 \div 5.0$ in the model with $\tau_B = 3$. The time-length of the first quasi-period falls, respectively, from $T_{\rm QP} \simeq 2.9$ to $T_{\rm QP} \simeq 2.1$. All the processes occurring at first stage and settling of the QPR are slower and less pronounced in the latter model.

The bar maximal amplitude ε_0 changing in rather wide range (we tried $\varepsilon_0 = 0.1$, $\varepsilon_0 = 0.3$ and $\varepsilon_0 = 0.5$) makes no essential difference in the results, though the mass and angular momentum flux densities grow and fall respectively. Nevertheless, Afanas'ev *et al.* (1989) show that the flux distributions are very different at $\varepsilon_0 = 0.05$. Perhaps, this value is a cut-off for the QPR which we discuss.

4.8 Disk Evolution after the Bar Turn-Off

We turned off abruptly (with a jump) the perturbing influence of the bar potential in an experiment with $\tau_B = 0.3$ and $\varepsilon_0 = 0.3$ at $t = 18$. That means that we took $\varepsilon(r, t > 18) = 0$ in Eq. 5.

After about 6 revolutions of the disk center since the bar turn-off the QP process dies away in the disk periphery ($r \gtrsim 2$). The large-scale nonaxisymmetric perturbations of considerable amplitude become axisymmetric with radial wavelength $1.5 \div 2$ and propagate outwards at the sound velocity. The small-scale ones degenerate into yet smaller scale waves of vanishing but finite amplitude. Later on, the wavelengths and amplitudes of axisymmetric perturbations decrease too.

We should note that after the QP process has decayed, the ring-like perturbations reach the grid's outer edge (cf. Figure 16) and reflect it. In a more realistic model of the disk without steep outer boundary a constructive interference is impossible, and thus, one can expect such perturbations to be damped in shorter times.

In the central part of the disk the bar turn-off means, first of all, that the potential saddle point disappears. Together with it the bisectorial structure of the flow is gone, because the gas outflow from the center is ceased while the inflow goes on, for the gas looses its angular momentum due to viscosity. So, the central depression of the gas surface density vanishes, and $\langle\sigma\rangle$ central peak grows monotonously (to the factor of 1.7 during 23 revolutions of the center after the bar turn-off), its typical diameter decreasing.

The disk as a whole evolves towards a quasi-state, with parameters changing under the influence of viscosity, as it occurs usually for the case of a single-peaked rotation curve decreasing outwards (see Gorbatski and Serbin, 1983; Gorbatski and

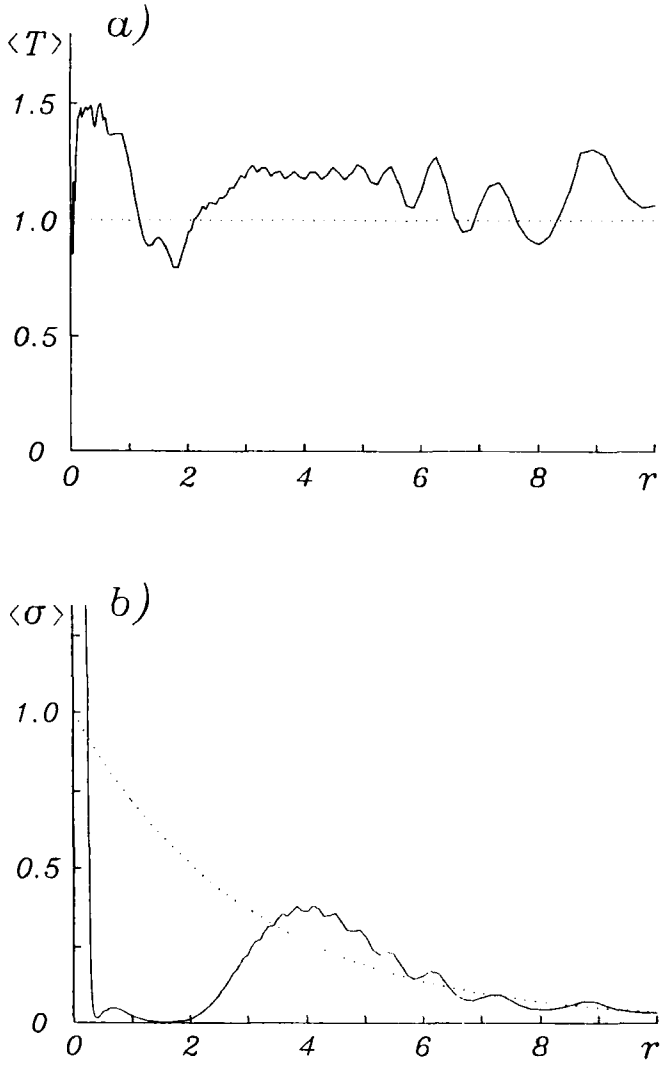

Figure 16 The radial distributions of temperature (*a*) and surface density (*b*) after 24 revolutions of the central region since the bar turn-off (solid lines). Dotted lines show the initial (at $t = 0$) distributions of the quantities.

Usovich, 1986). Meanwhile, the gas compression in the vicinity of the inner and the outer maxima of the surface density is accompanied by its heating despite the radiation losses (Figure 16). The radiation losses are the factor that allows the temperature exceeding the treshold value of T_0 to remain almost constant in time. The temperature oscillations in the outermost parts of the disk we think to be mainly the consequences of the boundary condition.

5 CONCLUSIONS

First of all, our results reveal a possibility of dynamic separation of the central and the peripheral regions – the rapidly growing bar just makes a "barrier" of surface density hollow, and afterwards the wave of potential associated with bar has a small influence upon the gas dynamics in the outer regions.

Formation of such a hollow of surface density between the central maximum near the nucleus and the outer molecular ring seems to be a common feature in the disks of flat galaxies of different types, since a very different disk evolution scenarios lead to it – see, e.g., Morozov *et al.* (1985c), Gorbatski and Serbin (1983), Gorbatski and Usovich (1986), Baev (1989), Zasov and Fridman (1987) and Fridman *et al.* (1990)†. This effect has to be more pronounced in barred galaxies.

Besides the minimum of $\langle\sigma\rangle$ close to the center (at $r \simeq 200$ pc), a hollow (depression) in surface density appears while the bar is growing and survives thereafter. It is similar to the one observed in many barred galaxies (and due to a saddle point of the gravitational potential).

The gaseous disk with rapidly growing bar passes through two stages of evolution. In the first stage there appears dynamic separation of the central and peripheral regions of the disk. In the second stage a quasiperiodic (auto-oscillatory) process sets up in the region outwards from the OLR.

The spiral-and-vortices patterns arising at these stages are generated by different ways, though they look very much alike. At the first stage, the growing wave of bar potential is responsible for the pattern development, and in the very QP the pattern is driven by the Kelvin–Helmholtz instability and centrifugal effects.

Although the gravitational potential is significantly non-axisymmetric, the axisymmetric mass and angular momentum transport are dominant.

If we suppose that, though some simplifying assumptions were made, our simulations give a qualitatively valid description of the processes in real objects, then the possibility seems to be interesting that a barred galaxy may change its morphological types. It may evolve consequently into spiral, ring and theta and theta-galaxy in very small times of about 10^8 years.

It seems to be very interesting that relative change in the gas rotation curve may reach $20 \div 30\%$ at $1 \leq r \leq 3$ kpc for a typical time of about 3×10^7 years, that is, during one revolution of the central part. Meanwhile, different features of the rotation curve appear and vanish, such as negative gradient, discontinuity of velocity, etc. (see Figure 13). But since the velocity dispersion of stars is large and angular momentum exchange between the stars and gas is relatively small, the rotation curve of stars must not deviate significantly from its equilibrium even if the gas self-gravity is included.

Since the gas rotation curve in a range of constant angular velocity exceeds the initial equilibrium one (i.e. determined by stars in the real disk) during all

†Note that similar density minimum appeared in numerical simulation of quasi-Keplerian accretion disks (Papaloizou and Savonije, 1991) due to the development of the spiral modes of resonantradiative instabilities.

simulation time, the dynamical friction effect must be significant at $r \leq 1$ kpc. This effect can affect the results. We expect the gas accretion rate and rotation velocity to grow and the surface density maximum to drift nearer to the center.

Finally, we point out possible consequences of the fact that, in reality, the stellar bar energy is finite. Freeman (1966a, b, c) and Hunter (1974) showed that losses of the bar angular momentum result in the bar major axis shortening and its rotation velocity growth. Our experiments show that, unlike the outer regions beyond the corotation radius, the energy and angular momentum exchange between the gas density wave and bar potential remains significant and never changes its sign in the central region during all simulation time. The faster the bar amplitude is growing in the first stage, the more intense the exchange is, and as a result, the more effective the bar shortening and speeding up goes. Since the relaxation processes must enhance the z-dispersion of the bar stars and distort the bar in the vertical direction, this may be viewed as a possible scenario of dynamic development of the bulge. An essential feature is that this scenario leads to H_2 regions distribution in the disk resembling the observed one (Sanders *et al.*, 1984). Note that Pfenninger and Norman (1990) made similar conclusions in their study of the accretion of molecular clouds onto a central mass concentration (numerically integrating the cloud orbits simulated with point particles of the corresponding mass; the weak dissipation was accounted for).

We believe that all the results given above indicate that a rapidly growing bar can lead to a bulge development, while the bar growing quasi-steadily may exist much longer – in times comparable with the Hubble time. This explains the existence of rapidly rotating bulges, elongated in the direction transverse to the bar major axis, observed in some SB galaxies (see, e.g., Gorbatski, 1986). Such bulges may be produced by the bar mode appeared at an earlier stage of the galaxy evolution, and the existing bars could arise much later. Since the spheroidal component affects the bar mode stabilizing it, the "secondary" bar orientation along the minor bulge axis is the most plausible.

The authors are grateful to Profs. V. G. Gorbatski, V. M. Kontorovich and Yu. M. Schekinov for their interest in this work and also to Drs. Yu. V. Mustsevaya. I. G. Kovalenko and A. V. Hoperskov for numerous helpful discussions. We deeply appreciate a number of valuable remarks of Profs. A. V. Zasov and A. G. Morozov.

The authors are grateful to the American Astronomical Society for financial support and to a Volgograd company "Sarmat-Union" for financial support which allowed to present our results at scientific meetings.

References

Afanas'ev, V. L., Levy, V. V., Morozov, A. G. (1989) *Preprint*, Volgograd State University, 6–89.
Athanassoula, E. (1980) *A. Ap.* **88**, 184.
Athanassoula, E. (1988) *Proc. "Intern. Scholl and Workshop on Plasma Astrophusics"*, Varenna.
Baev, P. V. (1989) Moscow, Moscow State University, Dis.kand.fiz.-mat.nauk.
Baker, P. L., Barker, P. K. (1974) *A. Ap.* **36**, 179,
Bochkarev, N. G. (1991) *Osnovy Fiziki Mezhzvezdnoy Sredy*, Moskow, Moskow UP, 352 p.

Belotserkovski, O. M., Davydov, Yu. M. *Method Krupnyh Chastits v Gazovoy Dinamike*, Moscow, Nauka, 349 p.
Churilov, S. M., Shukhman, I. G. (1981) *Astron. Tsirk.* **1157**, 1.
Fletcher, K. (1991) *Numerical Technics in Fluid Dynamics*, Moscow, Mir **1**, 504 p.
Freeman, K. C. (1966a) *MNRAS* **134**, 1.
Freeman, K. C. (1966b) *MNRAS* **134**, 15.
Freeman, K. C. (1966c) *MNRAS* **133**, 47.
Fridman, A. M. (1978) *Uspekhi Fiz. Nauk* **125**, 352.
Fridman, A. M. (1990) *Zhurn. Eksp. Teor. Fiz.* **98**, 1121.
Fridman, A. M., Polyachenko, V. L., Zasov, A. V. (1990) In *Dynamics of Galaxies and Molecular Cloud Distribution*, F. Combes and F. Casoli (eds.), Kluwer Academic Publishers, Dordrecht, Boston, London.
Fukunaga, M. (1983) *Publ. Astron. Soc. Jap.* **35**, 173.
Glatzel, W. (1987) *MNRAS* **225**, 227.
Glatzel, W. (1990) *MNRAS* **242**, 338.
Goldreich, P., Lynden–Bell, D. (1965) *MNRAS* **130**, 7.
Goldreich, P., Tremaine, S. (1982) *Ann. Rev. A. Ap.* **20**, 517.
Gorbatski, V. G. (1977) *Kosmicheskaya Gazodinamika*, Moscow, Nauka, 360 p.
Gorbatski, V. G. (1986) *Vvedenie v Fiziku Galaktik i Skoplenij Galaktik*, Moscow, Nauka, 256 p.
Gorbatski, V. G., Serbin, V. M. (1983) *Astrofizika* **19**, 79.
Gorbatski, V. G., Usovich, K. I. (1986) *Astrofizika* **25**, 125.
Hunter, C. (1974) *MNRAS* **166**, 633.
Korchagin, V. I., Shevelev, Yu. G. (1980) *Astrofizika* **16**, 757.
Korchagin, V. I., Shevelev, Yu. G. (1981) *Astrofizika* **17**, 455.
Kovalenko, I. G., Levy, V. V. (1992) *A. Ap.* **264**, 406.
Larson, R. B. (1988) In *The Formation and Evolution of Planetary Systems*, H. A. Weaver *et al.* (eds.), Cambridge UP.
Levy, V. V., Morozov, A. G. (1989) *Astrofizika* **30**, 371.
Levy, V. V. (1993) (in preparation).
Little, B., Carlberg, R. G. (1991) *MNRAS* **251**, 227.
Lipunov, V. M. (1982) *Astron. Zhurn.* **59**, 286.
Lynden–Bell, D., Kalnajs, A. J. (1972) *MNRAS* **157**, 1.
Marochnik, I. S., Berman, B., Mishurov, Yu. N., Suchkov, A. A. (1983) *Ap. S. Sci.* **89**, 177.
Matsuda, T., Inoue, M., Sawada, K., Shima, E., Wakamatsu, K. (1987) *MNRAS* **229**, 295.
Mikhajlova, E. A., Morozov, A. G. (1988) *Astron. Tsirk.* **1528**, 3.
Mishurov, Yu. N., Peftiev, V. I., Suchkov, A. A. (1976) *Astron. Zhurn.* **53**, 268.
Morozov, A. G. (1977) *Pis'ma Astron. Zhurn.* **3**, 195.
Morozov, A. G. (1979) *Astron. Zhurn.* **56**, 498.
Morozov, A. G. (1981) *Sov. Astron.* **25**, 421.
Morozov, A. G. (1989) *Kinematika i Fizika Nebesnyh Tel* **5**, 75.
Morozov, A. G., Hoperskov, A. V. (1990) *Pis'ma Astron. Zhurn.* **16**, 567.
Morozov, A. G., Mustsevoy, V. V., Prosvirov, A. E. (1992) *Pis'ma Astron. Zhurn.* **18**, 46.
Morozov, A. G., Nezlin, M. V., Snezhkin, E. N., Fridman, A. M. (1984) *Pis'ma Zhurn. Eksp. Teor. Fiz.* **39**, 504.
Morozov, A. G., Nezlin, M. V., Snezhkin, E. N., Fridman, A. M. (1985a) *Uspekhi Fiz. Nauk* **145**, 160.
Morozov, A. G., Nezlin, M. V., Snezhkin, E. N., Torgashin, Yu. M., Fridman, A. M. (1985b) *Astron. Tsirk.* **1414**, 1.
Morozov, A. G., Nezlin, M. V., Snezhkin, E. N., Torgashin, Yu. M., Fridman, A. M. (1985b) *Astron. Tsirk.* **1414**, 7.
Morozov, A. G., Torgashin, Yu. M., Fridman, A. M. (1986) *Nauch. Inform. Astron. Soveta AN SSSR* **61**, 110.
Mustsevoy, V. V., Prohorov, M. E. (1992) *Preprint*, Volgograd, Volgograd State University, 1–92.
Nezlin, M. V., Snezhkin, E. N. (1990) *Vikhri Rossbi i Spiral'nye Struktury*, Moscow, Nauka, 240 p.
Papaloizou, J. C. B., Pringle, J. E. (1985) *MNRAS* **213**, 799.
Papaloizou, J. C. B., Pringle, J. E. (1987) *MNRAS* **225**, 267.

Papaloizou, J. C. B., Savonije, G. J. (1991) *MNRAS* **248**, 353.
Pfenniger, D., Norman, C. (1990) *Ap. J.* **363**, 391.
Polyachenko, V. L., Fridman, A. M. (1976) *Ravnovesie i Ustoychivost' Gravitiruschih System*, Moscow, Nauka, 447 p.
Roberts, W. N. Jr., Hausman, M. A. (1984) *Ap. J.* **277**, 74.
Roberts, W. W. (1969) *Ap. J.* **158**, 123.
Sanders, P. B., Solomon, P. M., Scoville, N. Z. (1984) *Ap. J.* **276**, 182.
Savonije, G. J., Heemskerk, M. H. M. (1990) *A. Ap.* **240**, 191.
Saslaw, W. (1989) *Gravitational Physics of Stellar and Galactic Systems*, Moscow, Mir, 544 p.
Sawada, K., Matsuda, T., Inoue, M., Hachisu, I. (1987) *MNRAS* **224**, 307.
Sellwood, J. A. (1980) *A. Ap.* **89**, 296.
Sil'chenko, O. K., Lipunov, V. M. (1987) *Astrofizika* **26**, 363.
Sil'chenko, O. K., Lipunov, V. M. (1987) *Astrofizika* **26**, 443.
Spruit, H. (1989) In *Theory of Accretion Disks*, F. Meyer, W.-J, Duschl, J. Frank, and E. Meyer-Hofmeister (eds.), Kluwer Academic Publishers, Dordrecht, 325.
Surdin, V. G. (1980) *Astron. Tsirk.* **1113**, 3.
Toomre, A. (1964) *Ap. J.* **139**, 1217.
Toomre, A. (1977) *Ann. Rev. A. Ap.* **15**, 437.
Toomre, A. (1981) In *The Structure and Evolution of Normal Galaxies*, S. M. Fall and D. Lynden-Bell (eds.), Cambridge UP.
Usovich, K. I. (1988) *Astrofizika* **28**, 510.
van Albada, T. S., Sanders, R. H. (1982) *MNRAS* **198**, 865.
Zasov, A. V., Fridman, A. M. (1987) *Astron. Tsirk.* **1519**, 1.